

A laminated composite plate finite element *a-priori* corrected for locking

João Elias Abdalla Filho[†]

Programa de Pós-Graduação em Engenharia Mecânica, Pontifícia Univ Católica do Paraná (PUCPR)
Rua Imaculada Conceição, 1155- Prado Velho - 80215-901, Curitiba - PR, Brasil
Curso de Engenharia de Produção Civil, Universidade Tecnológica Federal do Paraná (UTFPR)
Rua Sete de Setembro, 3165 – Centro – 80000-000, Curitiba – PR, Brasil

Ivan Moura Belo and Michele Schunemann Pereira

Programa de Pós-Graduação em Engenharia Mecânica, Pontifícia Univ Católica do Paraná (PUCPR)
Rua Imaculada Conceição, 1155- Prado Velho - 80215-901, Curitiba - PR, Brasil

(Received October 10, 2006, Accepted January 8, 2008)

Abstract. A four-node plate finite element for the analysis of laminated composites which is developed using strain gradient notation is presented. The element is based on a first-order shear deformation theory and on the equivalent lamina assumption. Strains and stresses can be calculated at different points through the thickness of the plate. They are averaged values due to the equivalent lamina assumption. A shear correction factor is used as the transverse shear strain is taken to be constant over the plate thickness while its actual variation is parabolic. Strain gradient notation, which is physically interpretable, allows for the detailed *a-priori* analysis of the finite element model. The polynomial expansions are inspected and spurious terms responsible for modeling errors are identified in the shear strains polynomial expansions. The element is corrected by simply removing the spurious terms from the shear strains expansions. The element is implemented into a FORTRAN finite element code in two versions; namely, with and without spurious terms. Results are compared to show the effects of the spurious terms on the solutions. It is also shown that a refined mesh composed of corrected elements provides solutions which approximate very well the analytical solutions, validating the procedure.

Keywords: laminated composites; plates; finite elements; locking; strain gradient notation; parasitic shear.

1. Introduction

This work proposes a four-node rectangular finite element for the analysis of laminated composite plates, which is developed using strain gradient notation. The element is based on a first-order shear deformation theory, which considers the transverse shear strains according to Mindlin's theory. The element is also based on the equivalent lamina assumption, which treats the laminate as one single,

[†] Professor, Corresponding author, E-mail: joao.abdalla@pucpr.br

orthotropic lamina plate whose constitutive properties are the average of the properties of all laminae.

Strain gradient notation consists in an alternative notation for writing finite element polynomials. Strain gradient notation is a physically interpretable notation which relates displacements to the kinematic quantities of the continuum. The identification of this relationship is possible due to a procedure which identifies the physical contents of the polynomial coefficients (Dow 1999). The main advantage of the use of such a notation is that the modeling characteristics of the finite element are made clear since the early steps of the formulation. Thus, sources of modeling errors can be identified and also removed from the finite element polynomial expansions prior to the formation of its stiffness matrix.

Strain gradient notation has been employed to analyze various problems in structural mechanics. The early application was in the description of the behavior of lattice structures (Dow *et al.* 1985, Dow and Hyuer 1989). Next, the notation was employed to formulate stiffness matrices of plane elasticity finite elements (Dow *et al.* 1985, Dow and Byrd 1988) where it was recognized the possibility of precisely and physically identifying the erroneous terms which are responsible for parasitic shear. A procedure for eliminating those spurious terms has been easily established. Then, the use of strain gradient notation was extended to beam and plate analysis where a procedure to remove or at least reduce the effects of shear locking was devised (Dow and Byrd 1988, Dow and Byrd 1990). Further, it was applied in the analysis of laminated composite structures where qualitative errors were identified (Abdalla 1992, Dow and Abdalla 1994, Abdalla and Dow 1994). In the latter, laminated composite plate elements were formulated and modeling error analyses were performed. That is, spurious terms present in the elements shear strains polynomial expansions were identified and their effects in the performance of the elements were investigated. It was determined that spurious terms were able to interfere with the correct representation of mode coupling of non-symmetric laminates. Further, that refinement was not always able to attenuate the effects of the spurious terms, enforcing the need to remove them prior to numerical analyses. Those works were not however concerned with validating the elements for stresses computation. The present work is therefore filling a gap as it validates the four-node laminated composite plate element by comparing numerical stresses solutions to analytical stresses solutions.

Elimination of locking in finite element analysis of plates and shells has been a major concern for many decades. As the literature is vast in this field, we will not attempt to make a thorough review, but will make reference to a few important works, mostly those concerned with four-noded elements. A pioneering work of Zienkiewicz and co-workers (Zienkiewicz *et al.* 1971) recognizes that an element derived earlier (Ahmad *et al.* 1970) increases unduly in stiffness for thin problems. Recognizing the phenomenon as parasitic shear, they apply a reduced-order integration to calculate transverse shear stresses, obtaining acceptable results. Hughes and co-workers (Hughes *et al.* 1977) use one-point quadrature to integrate the shear energy to avoid locking in a regular four-node C^0 -continuity plate element (bilinear element) when analyzing thin plates. A follow-up work (Hughes *et al.* 1978) addresses reduced and selective reduced integration of plate elements. Among many positive conclusions, the authors point out the negative aspect that zero energy modes (rank deficiency) cannot be eliminated completely through those techniques, and that the adding of incompatible modes to the bilinear element does not provide satisfactory results. A four-node plate element is devised which does not contain spurious zero energy modes, passes the patch test and does not lock when applied to thin problems (Bathe and Dvorkin 1985). The element is based on Mindlin/Reissner plate theory and assumes a transverse shear strain field. Another author (Prathap

1997) uses the field-consistency approach to demonstrate the sources of locking in the four-node Mindlin plate element and to explain why one-point Gaussian integration is not able to remove locking when the plate gets thicker. Further, he proposes selective reduced integration strategies to remove locking from the thick element.

In this work, the spurious terms which are present in the shear strain polynomial expansions of the proposed element are identified. It is demonstrated both theoretically and numerically that they are flexural terms which cause stiffening of the model by increasing the element's shear strain energy when bending of the plate occurs. Mesh refinement reduces the locking effects of the spurious terms and, eventually, it might be able to remove them. Here, after their precise identification, which is done by inspection, the spurious terms are removed from the shear strain expressions, rendering a corrected element for locking. Therefore, locking is taken care *a-priori* of the formation of the stiffness matrix and of the computer implementation such that no numerical technique need be employed during analysis to remove it.

Research on analytical and numerical modeling of laminated composites has been very active in order to achieve accurate representation of the actual behavior of this kind of structures. A very thorough review on theories for isotropic and anisotropic laminated plates is performed, citing over four hundred references (Ghugal and Shimpi 2002). An also thorough review on theories and computational models for laminated composites is presented (Reddy and Averill 1991). That review has been updated more recently (Reddy 2004).

High-order deformation theories have been proposed in several works (Lo *et al.* 1977, Singh and Rao 1995, Bose and Reddy 1998) among others. An interesting work (Reddy and Wang 2000) presents an overview of the relationships between classical and shear deformation theories. Computational models ranging from simple to refined which allow for numerical evaluation of all those theories have been developed (Reddy 1989, Bose and Reddy 1998). Further, a layerwise model is proposed where locking is avoided by prescribing a transverse shear deformation field compatible with the assumed displacement field (Botello *et al.* 1999). A four-noded mixed finite element for composites is developed which is based on the work of Bathe and Dvorkin (Brank and Carrera 2000). A triangular element for composites is developed which is based on Reddy's simple higher-order shear deformation theory (Sheikh and Chakrabarti 2003). The element is free of locking and does not contain any spurious modes. Reddy's displacement for third order shear deformation theory is employed to derive a set of equations to model the behavior of laminated plates. A triangular finite element is implemented using those equations (Agaah *et al.* 2003).

In spite of all the advances in the numerical analysis of laminated composites, this paper addresses the formulation and performance of a first-order shear deformation theory element and demonstrates an alternative procedure to identify and eliminate the sources of locking. The element is implemented in a FORTRAN finite element code in both versions, that is, with the spurious terms and after their elimination. Comparison of numerical results show how the spurious terms stiffens the model, requiring more refined meshes in order to attain convergence. Also, the corrected model is validated by comparing numerical solutions with results obtained from analytical solutions (Reddy 2004).

2. Theoretical description

For completeness, this section presents the macromechanical theory adopted to describe laminated

composites as well as the necessary expressions pertaining to Mindlin's theory of plates. Also, strain gradient notation is introduced into the formulation of the laminate prompting it for finite element development.

The macromechanical theory for laminated composite plates adopted here is based on the following assumptions: (1) Plane sections normal to the middle surface of the plate remain plane, but not necessarily normal after bending. Thus, the model accounts for transverse shear deformation of the plate; (2) There is a perfect bond between laminae, preventing relative slippage. That is, the behavior of the laminate may be represented by the behavior of its middle surface, and laminae compatibility is imposed; and (3) Normal-to-the-middle-surface components of stress and strain are negligible, not being included in the model.

The laminate has the capability of developing in-plane displacements u and v along the x and y directions, respectively; out-of-plane displacements w , and rotations q and p in the x and y directions, respectively (or around the y and x axes, respectively). The displacements w are independent of rotations q and p , allowing for transverse shear deformation. The kinematic relations of the plate are the following

$$u(x, y, z) = u_0(x, y) + zq(x, y) \quad (1)$$

$$v(x, y, z) = v_0(x, y) - zp(x, y) \quad (2)$$

$$w(x, y) = w \quad (3)$$

$$q(x, y) = \frac{\partial u(x, y, z)}{\partial z} \quad (4)$$

$$p(x, y) = -\frac{\partial v(x, y, z)}{\partial z} \quad (5)$$

where u_0 and v_0 are middle surface in-plane displacements, and z is the coordinate which is associated to the thickness of the plate.

The strains are arranged in vector form as shown below

$$\begin{Bmatrix} \varepsilon_x \\ \varepsilon_y \\ \gamma_{xy} \\ \gamma_{yz} \\ \gamma_{xz} \end{Bmatrix} = \begin{Bmatrix} u_{o,x} \\ v_{o,y} \\ u_{o,y} + v_{o,x} \\ 0 \\ 0 \end{Bmatrix} + \begin{Bmatrix} zq_{,x} \\ -zp_{,y} \\ z(q_{,y} - p_{,x}) \\ w_{,y} - p \\ w_{,x} + q \end{Bmatrix} \quad (6)$$

where the first vector contains membrane strains and the second vector contains plate bending strains.

The strain energy of the laminate is the sum of the strain energies of its laminae. Hence

$$U = \frac{1}{2} \sum_{k=1}^n \int_{\Omega_k} \{\varepsilon\}_k^T [Q]_k \{\varepsilon\}_k d\Omega_k \quad (7)$$

where k is a typical lamina, n is the total number of laminae, $\{\varepsilon\}_k$ is the strain vector of lamina k , $[Q]_k$ is the constitutive properties matrix of lamina k , and Ω_k is the volume of lamina k .

At this point, strain gradient notation is introduced into the formulation. Displacements are related to kinematic quantities of the continuum, which are rigid body modes, strains, and first-order and higher-order derivatives of strains. These kinematic quantities are generally referred to as strain gradients. The relations of displacements and strains to strain gradients are given, respectively, by

$$\{d\} = [\phi]\{\varepsilon_{sg}\} \tag{8}$$

$$\{\varepsilon\} = [T_{sg}]\{\varepsilon_{sg}\} \tag{9}$$

where $[\phi]$ and $[T_{sg}]$ are the corresponding transformation matrices, and $\{\varepsilon_{sg}\}$ is the strain gradients vector. This vector contains the set of independent deformation modes that the model is capable of representing. Matrix $[\phi]$ is comprised of linearly independent vectors, each associated to a strain gradient component, describing a specific deformation pattern of the model. Eqs. (8) and (9) are combined to eliminate vector $\{\varepsilon_{sg}\}$. The result is substituted into Eq. (7) to yield

$$U = \frac{1}{2}\{d\}^T[\phi]^{-T}\left(\sum_{k=1}^n \int_{\Omega_k} [T_{sg}]_k^T [Q]_k \{T_{sg}\}_k d\Omega_k\right)[\phi]^{-1}\{d\} \tag{10}$$

which is an expression of the strain energy in *strain gradient* notation. The quantity between parentheses is called strain energy matrix and it is represented by $[U_M]$. The elements of its principal diagonal contain the quantities of strain energy associated with the pure strain modes of the laminate. The other elements of the matrix contain the quantities of energy associated with the coupling between the various strain modes. Matrix $[U_M]$ may be written as

$$[U_M] = \int \sum_{k=1}^n \int_{z_{k-1}}^{z_k} [T_{sg}]_k^T [Q]_k [T_{sg}]_k dZ_k dA \tag{11}$$

where the volume integral has been broken into an integral over the area of the middle surface of the laminate and an integral over its thickness. This line integral is carried out as the sum of the integrals over the thicknesses of the various laminae. The integration limits z_{k-1} e z_k represent the bottom and top coordinates of a typical lamina k respectively. The integration over the thickness of the laminate yields its stiffness quantities

$$A_{ij} = \sum_{k=1}^n (Q_{ij})_k (Z_k - Z_{k-1}) \tag{12}$$

$$B_{ij} = \frac{1}{2} \sum_{k=1}^n (Q_{ij})_k (Z_k^2 - Z_{k-1}^2) \tag{13}$$

$$D_{ij} = \frac{1}{3} \sum_{k=1}^n (Q_{ij})_k (Z_k^3 - Z_{k-1}^3) \tag{14}$$

$$A_{ij}^* = K \sum_{k=1}^n (Q_{ij})_k (Z_k - Z_{k-1}) \tag{15}$$

where A is the membrane stiffness, B is the membrane-bending coupling stiffness, D is the bending stiffness, and A^* is the membrane stiffness associated to the effects of transverse shear subjected to the shear correction factor K . According to Reddy (2004), the determination of the shear correction

factor for laminates is still an unresolved issue. It depends on lamination scheme, geometry, and material properties. The most commonly used value for K is $5/6$, which can be demonstrated to be very accurate for homogeneous, isotropic plates. This value is employed by the analytical solutions (Reddy 2004) which are used to validate the proposed element. Therefore, this same value is adopted in the numerical solutions performed here for consistency.

Finally, the general expression of the stiffness matrix in strain gradient notation is determined recalling the definition of strain energy in terms of the stiffness matrix

$$U = \frac{1}{2} \{d\}^T [K] \{d\} \quad (16)$$

and comparing this equation to Eq. (10) after inserting Eq. (11) into the latter

$$[K] = [\phi]^{-T} [U_M] [\phi]^{-1} \quad (17)$$

3. Finite element model

This section presents the development of the four-node rectangular plate finite element in strain gradient notation. The element has five degrees of freedom at each node, namely; the in-plane displacements u and v , the out-of-plane displacement w , and the rotations p and q around the x and y axes, respectively, as shown in Fig. 1. The essential field variables of the problem are the in-plane displacements u and v , and the out-of-plane displacement w . Polynomials for these variables must be built to start the finite element formulation. Next, definitions in Eqs. (4) and (5) must be employed to define the polynomials representing rotations q and p .

In strain gradient notation these polynomials are

$$u(x, y, z) = (u)_o + (\varepsilon_x)_o x + (\gamma_{xy}/2 - r)_o y + (\varepsilon_{x,y})_o xy + (\gamma_{xz}/2 + q)_o z \\ + (\varepsilon_{x,z})_o xz + (\varepsilon_{x,yz})_o xyz + ((\gamma_{xy,z} - \gamma_{yz,x} + \gamma_{xz,y})/2)_o yz \quad (18)$$

$$v(x, y, z) = (v)_o + (\gamma_{xy}/2 + r)_o x + (\varepsilon_y)_o y + (\varepsilon_{y,x})_o xy + (\gamma_{yz}/2 - p)_o z \\ + (\varepsilon_{y,z})_o yz + (\varepsilon_{y,xz})_o xyz + ((\gamma_{xy,z} + \gamma_{yz,x} - \gamma_{xz,y})/2)_o xz \quad (19)$$

$$w(x, y) = (w)_o + (\gamma_{xz}/2 - q)_o x + (\gamma_{yz}/2 + p)_o y + ((-\gamma_{xy,z} + \gamma_{yz,x} + \gamma_{xz,y})/2)_o xy \quad (20)$$

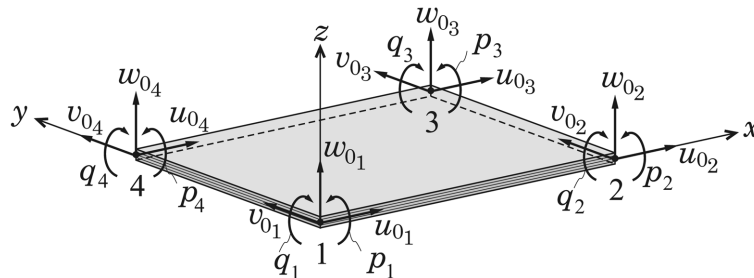


Fig. 1 Four-node rectangular plate finite element

$$q(x, y) = (\gamma_{xz}/2 + q)_o + (\varepsilon_{x,z})_o x + ((\gamma_{xy,z} - \gamma_{yz,x} + \gamma_{xz,y})/2)_o y + (\varepsilon_{x,yz})_o xy \quad (21)$$

$$p(x, y) = (p - \gamma_{yz}/2)_o + ((-\gamma_{xy,z} - \gamma_{yz,x} + \gamma_{xz,y})/2)_o x + (-\varepsilon_{y,z})_o y + (-\varepsilon_{y,xz})_o xy \quad (22)$$

These expressions have been originally developed in (Abdalla 1992). The procedure is performed here in detail as it is unknown to most readers. The middle surface in-plane displacements, the out-of-plane displacement and the rotations are initially written in terms of unknown coefficients.

$$u_o(x, y) = a_0 + a_1 x + a_2 y + a_3 xy \quad (23)$$

$$v_o(x, y) = b_0 + b_1 x + b_2 y + b_3 xy \quad (24)$$

$$w(x, y) = c_0 + c_1 x + c_2 y + c_3 xy \quad (25)$$

$$q(x, y) = d_0 + d_1 x + d_2 y + d_3 xy \quad (26)$$

$$p(x, y) = e_0 + e_1 x + e_2 y + e_3 xy \quad (27)$$

These polynomials are evaluated at the origin of the element, defining the contents of the independent terms of the expressions above

$$a_0 = (u)_o \quad (28)$$

$$b_0 = (v)_o \quad (29)$$

$$c_0 = (w)_o \quad (30)$$

$$d_0 = (q)_o \quad (31)$$

$$e_0 = (p)_o \quad (32)$$

Next, the in-plane normal strains ε_x and ε_y are written according to the definitions in Eq. (6) and are evaluated at the origin of the element, yielding

$$a_1 = (\varepsilon_x)_o \quad (33)$$

$$b_2 = (\varepsilon_y)_o \quad (34)$$

Then the in-plane shear strain γ_{xy} is written according to the definition in Eq. (6) and the in-plane rotation is written according to the definition below

$$r = \frac{1}{2} \left(\frac{\partial v}{\partial x} - \frac{\partial u}{\partial y} \right) \quad (35)$$

and are evaluated at the origin of the element producing two equations that are solved simultaneously to give

$$a_2 = \frac{1}{2} (\gamma_{xy})_o - (r)_o \quad (36)$$

$$b_1 = \frac{1}{2} (\gamma_{xy})_o + (r)_o \quad (37)$$

Proceeding on the transverse shear strains γ_{xz} and γ_{yz} are written according to the definitions in Eq. (6) and produce the coefficients below after being evaluated at the origin of the element

$$c_1 = (\gamma_{xz})_o - (q)_o \quad (38)$$

$$c_2 = (\gamma_{yz})_o + (p)_o \quad (39)$$

Next derivatives of normal strains or normal strain gradients $\varepsilon_{x,y}$, $\varepsilon_{y,x}$, $\varepsilon_{x,z}$ and $\varepsilon_{y,z}$ are written, and are evaluated at the origin of the element, resulting in the following coefficients

$$a_3 = (\varepsilon_{x,y})_o \quad (40)$$

$$b_3 = (\varepsilon_{y,x})_o \quad (41)$$

$$d_1 = (\varepsilon_{x,z})_o \quad (42)$$

$$e_2 = (\varepsilon_{y,z})_o \quad (43)$$

Also derivatives of shear strains or shear strain gradients $\gamma_{xy,z}$, $\gamma_{yz,x}$ and $\gamma_{xz,y}$ are written, and are evaluated at the origin producing three equations which are solved simultaneously, providing the following coefficients

$$c_3 = \frac{1}{2}(-\gamma_{xy,z} + \gamma_{xz,y} + \gamma_{yz,x})_o \quad (44)$$

$$d_2 = \frac{1}{2}(\gamma_{xy,z} + \gamma_{xz,y} - \gamma_{yz,x})_o \quad (45)$$

$$e_2 = \frac{1}{2}(-\gamma_{xy,z} + \gamma_{xz,y} - \gamma_{yz,x})_o \quad (46)$$

Finally second derivatives of normal strains $\varepsilon_{x,yz}$ and $\varepsilon_{y,xz}$ are written and evaluated at the origin of the finite element to define the last two coefficients

$$d_3 = (\varepsilon_{x,yz})_o \quad (47)$$

$$e_3 = (\varepsilon_{y,xz})_o \quad (48)$$

The coefficients are then backsubstituted into Eq. (23) through Eq. (27), which in turn are employed along with the kinematic relations of the plate, Eq. (1) through Eq. (5), to provide the finite element approximating functions in terms of strain gradients, Eq. (18) through Eq. (22).

Now that the procedure to obtain the approximating functions in terms of strain gradients has been detailed, these expressions are inspected showing that the displacements are comprised of terms which are functions of rigid body modes, constant normal and shear strains, and first and second-order derivatives of normal and shear strains. These quantities comprise the set of twenty strain gradients that form the deformation basis of the four-noded plate model, and they are listed below

$(u)_o, (v)_o, (w)_o, (r)_o, (p)_o, (q)_o$ - rigid body modes

$(\varepsilon_x)_o, (\varepsilon_y)_o, (\gamma_{xy})_o, (\gamma_{yz})_o, (\gamma_{xz})_o$ - constant strain modes

$(\varepsilon_{x,y})_o, (\varepsilon_{x,z})_o, (\varepsilon_{y,x})_o, (\varepsilon_{y,z})_o$ - first-order normal strain gradients

$(\gamma_{xy,z})_o, (\gamma_{yz,x})_o, (\gamma_{xz,y})_o$ - first-order shear strain gradients

$(\varepsilon_{x,yz})_o, (\varepsilon_{y,xz})_o$ - second-order normal strain gradients

Applying the definitions of the theory of elasticity, the strain polynomial expansions result:

$$\varepsilon_x = (\varepsilon_x)_o + (\varepsilon_{x,y})_o y + (\varepsilon_{x,z})_o z + (\varepsilon_{x,yz})_o yz \quad (49)$$

$$\varepsilon_y = (\varepsilon_y)_o + (\varepsilon_{y,x})_o x + (\varepsilon_{y,z})_o z + (\varepsilon_{y,xz})_o xz \quad (50)$$

$$\gamma_{xy} = (\gamma_{xy})_o + (\varepsilon_{x,y})_o x + (\varepsilon_{y,x})_o y + (\gamma_{xy,z})_o z + (\varepsilon_{y,xz})_o yz + (\varepsilon_{x,yz})_o xz \quad (51)$$

$$\gamma_{yz} = (\gamma_{yz})_o + (\gamma_{yz,x})_o x + (\varepsilon_{y,z})_o y + (\varepsilon_{y,xz})_o xy \quad (52)$$

$$\gamma_{xz} = (\gamma_{xz})_o + (\gamma_{xz,y})_o y + (\varepsilon_{x,z})_o x + (\varepsilon_{x,yz})_o xy \quad (53)$$

Strain gradient notation, which is physically interpretable, allows for an *a-priori* evaluation of the modeling capabilities of the finite element. Eq. (49) and Eq. (50) show that the normal strain expansions contain only strain states which are associated to the corresponding normal strains. All the coefficients are terms of the corresponding Taylor series expansions. However, the expansions for shear strains, Eq. (51), Eq. (52) and Eq. (53), contain terms which do not belong to their expansions in Taylor series; namely, the first and second-order derivatives of normal strains. That is, the following six strain states: $(\varepsilon_{x,y})_o, (\varepsilon_{x,z})_o, (\varepsilon_{y,x})_o, (\varepsilon_{y,z})_o, (\varepsilon_{x,yz})_o, (\varepsilon_{y,xz})_o$. These spurious terms may be called *parasitic shear* because they increase the shear strain energy of the element unduly when they are activated during the element's deformation. That is, they are the cause of shear locking. The reason for the presence of spurious terms is the use of *inconsistent* polynomials for displacement w and rotations p and q . For consistency, the polynomial for w must be one order higher than the polynomials for p and q because the transverse shear strains are defined as the sum of rotations and first derivatives of the out-of-plane displacement. In the present case, all three polynomials are of the same order. In order to correct the element, these spurious terms are removed from the shear strain polynomial expansions, resulting in the following expressions

$$\gamma_{xy} = (\gamma_{xy})_o + (\gamma_{xy,z})_o z \quad (54)$$

$$\gamma_{yz} = (\gamma_{yz})_o + (\gamma_{yz,x})_o x \quad (55)$$

$$\gamma_{xz} = (\gamma_{xz})_o + (\gamma_{xz,y})_o y \quad (56)$$

Computationally, the presence or the elimination of the spurious terms is accounted for in matrix $[T_{sg}]$ (see Eq. (9)), which in turn affects the values of stiffness components as shown in the expression of the stiffness matrix in strain gradient notation defined by Eq. (17) and repeated below

$$[K] = [\phi]^{-T} \int_A \left(\sum_{k=1}^n \int_{z_{k-1}}^{z_k} [T_{sg}]_k^T [Q]_k [T_{sg}]_k dz_k \right) dA [\phi]^{-1} = [\phi]^{-T} [U_M] [\phi]^{-1} \quad (57)$$

It will be shown in the next section that the activation of some or all of these spurious terms

causes severe locking of the model, requiring refinement effort for the model to attain convergence. On the other hand, it will be shown that by simply removing those terms from the shear strain expansions locking is eliminated.

The authors would like to make the observation that the element is not formulated using the isoparametric formulation. Therefore, the element is not designed to assume arbitrary shapes. Although this may be viewed as limiting, numerical examples presented below demonstrate that the element behaves quite well for regular geometries after elimination of the spurious terms, which is a main purpose of this paper. Further, stresses are always calculated at the nodes in both versions of the element, with and without spurious terms. Gauss points are not used in the present analyses.

4. Numerical applications

In this section, three different problems are solved using the model described above. The plates analyzed are all rectangular and their sides are nominated a and b if parallel to the x and the y -axis, respectively. Different lamination schemes, loading and boundary conditions are employed. Also, the thicknesses h of the plates change. Lower and higher thickness laminates are analyzed. All layers are of graphite-epoxy with the following mechanical properties: $E_x = 175$ GPa, $E_y = 175$ GPa, $G_{xy} = 3.5$ GPa, $G_{xz} = 3.5$ GPa, $G_{yz} = 1.4$ GPa, $\nu_{xy} = 0.25$. All problems are solved using five uniform meshes; namely, 2×2 , 4×4 , 8×8 , 16×16 , and 32×32 , both with elements containing the spurious terms (parasitic shear terms), and with corrected elements. Numerical solutions are compared among themselves to show the deleterious effects (locking) of the spurious terms. Further, these solutions are compared with analytical solutions whenever such solutions are available to show the effectiveness of the proposed model. Analytical solutions are constructed using solutions derived by Reddy (2004). Stresses results are made non-dimensional through the following relations (Reddy 2004)

$$\begin{aligned} \bar{\sigma}_{xx} &= \sigma_{xx} \left(\frac{h^2}{a^2 q_0} \right) & \bar{\sigma}_{yy} &= \sigma_{yy} \left(\frac{h^2}{a^2 q_0} \right) & \bar{\tau}_{xy} &= \tau_{xy} \left(\frac{h^2}{a^2 q_0} \right) \\ \bar{\tau}_{xz} &= \tau_{xz} \left(\frac{h^2}{aq_0} \right) & \bar{\tau}_{yz} &= \tau_{yz} \left(\frac{h^2}{aq_0} \right) \end{aligned} \quad (58)$$

Furthermore, in the plots that depict the various solutions that follow, FSDT is the analytical solution for the first-order shear deformation theory to which the numerical solutions are being compared. The numerical solutions containing spurious terms (parasitic shear) are referred to as with PS while those not containing spurious terms are referred to as wout PS. The plots also show the side length-to-thickness relation a/h , and the lamination scheme of the laminate. Percent errors in the highest values of stresses provided by the numerical analyses are calculated with respect to the analytical values and tabulated (Table 1, Table 2, and Table 3). Those percent errors help in quantifying the accuracies of the numerical solutions.

4.1 Problem #1

The first problem is a square simply supported cross-ply laminated composite plate subjected to a uniform load of value $q_0 = 10$ N/m². The laminate is symmetric with lamination scheme $0^\circ/90^\circ/90^\circ/$

0° , and the sides of the laminate are 1.0 m in length ($a = b = 1.0$ m). The plate is solved both with side-to-thickness ratios $a/h = 10$ and $a/h = 100$. In-plane normal stresses σ_{xx} and σ_{yy} are calculated at the center point of the plate, while transverse shear stresses τ_{xz} and τ_{yz} are calculated at the borders middle points.

First, solutions for the higher thickness plate ($a/h = 10$) are presented. Fig. 2(a) through Fig. 2(l) show the results of those analyses. Fig. 2(a) and Fig. 2(b) show the σ_{xx} solutions with and without the spurious terms, respectively, while Fig. 2(c) and Fig. 2(d) show the σ_{yy} solutions with and without the spurious terms, respectively. These figures show that the effects of the spurious terms are not very important in the in-plane stresses solutions. Such effects are only evident in the coarse meshes solutions and are rapidly eliminated by refinement. All four models converge to the

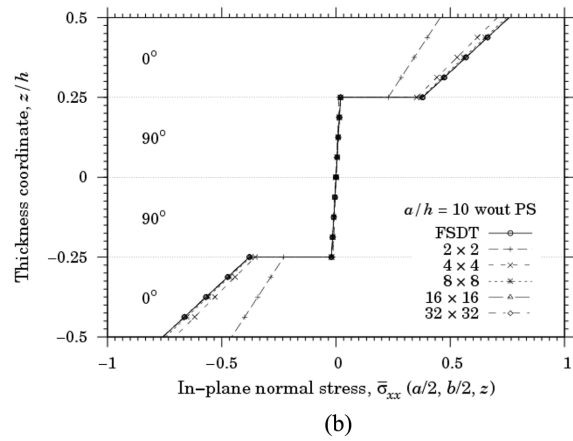
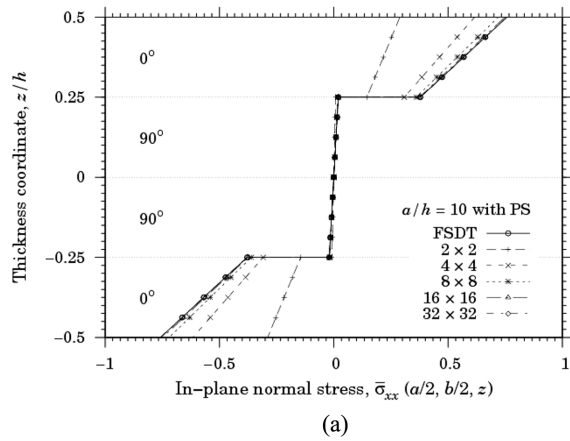


Fig. 2(a) Symmetric cross-ply laminate with side-to-thickness ratio $a/h = 10$. Normal stresses σ_{xx} computed through the thickness of the laminate with spurious terms

Fig. 2(b) Symmetric cross-ply laminate with side-to-thickness ratio $a/h = 10$. Normal stresses σ_{xx} computed through the thickness of the laminate without spurious terms

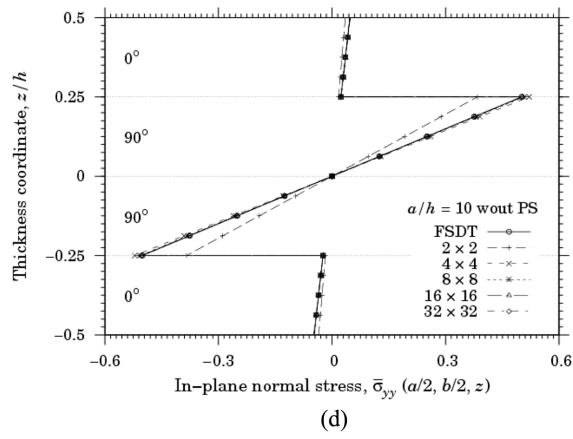
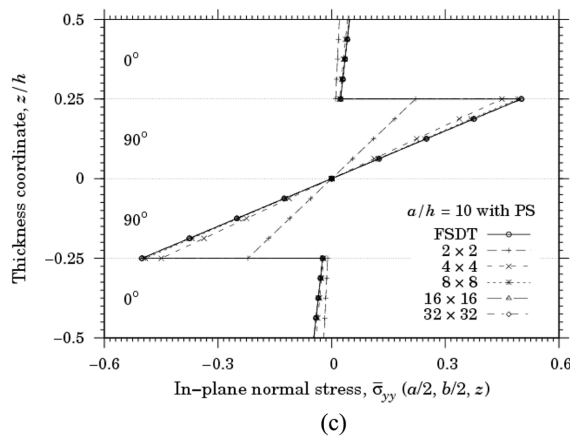


Fig. 2(c) Symmetric cross-ply laminate with side-to-thickness ratio $a/h = 10$. Normal stresses σ_{yy} computed through the thickness of the laminate with spurious terms

Fig. 2(d) Symmetric cross-ply laminate with side-to-thickness ratio $a/h = 10$. Normal stresses σ_{yy} computed through the thickness of the laminate without spurious terms

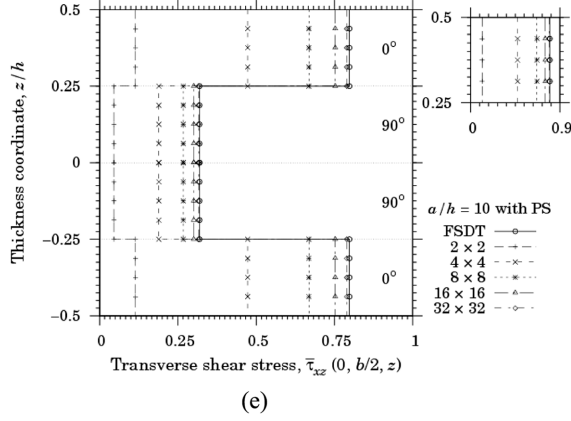


Fig. 2(e) Symmetric cross-ply laminate with side-to-thickness ratio $a/h = 10$. Transverse shear stresses τ_{xz} computed through the thickness of the laminate with spurious terms

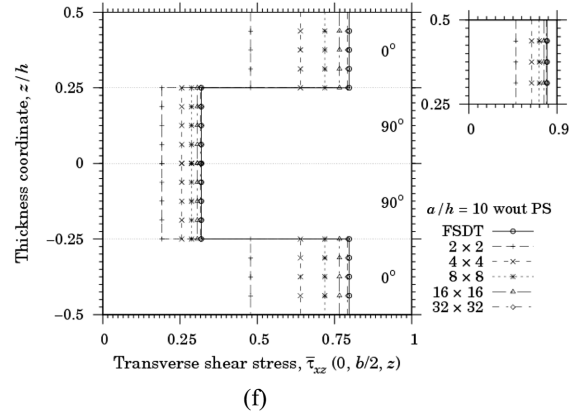


Fig. 2(f) Symmetric cross-ply laminate with side-to-thickness ratio $a/h = 10$. Transverse shear stresses τ_{xz} computed through the thickness of the laminate without spurious terms

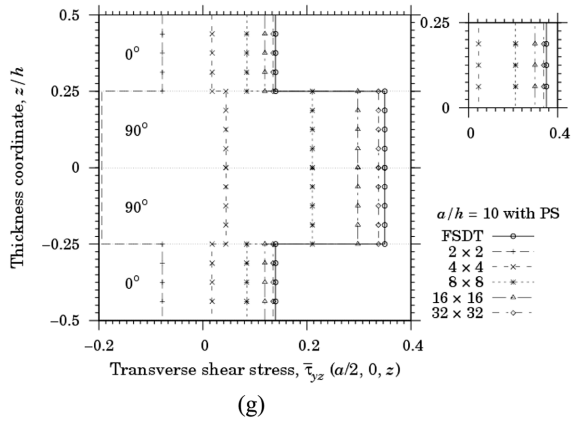


Fig. 2(g) Symmetric cross-ply laminate with side-to-thickness ratio $a/h = 10$. Transverse shear stresses τ_{yz} computed through the thickness of the laminate with spurious terms

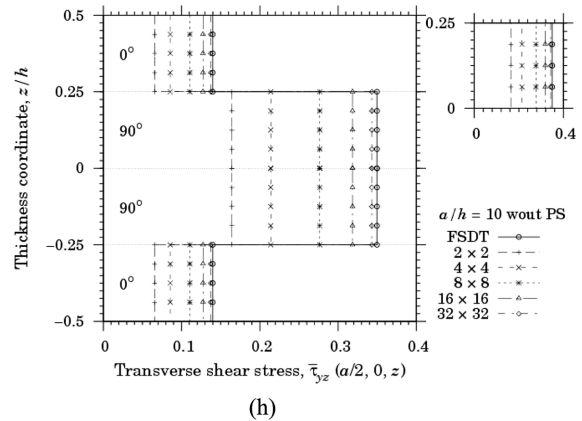
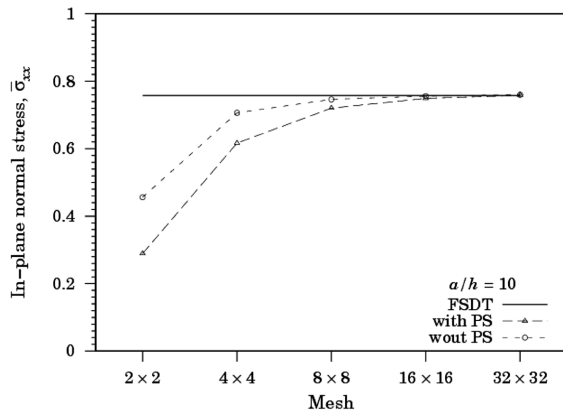


Fig. 2(h) Symmetric cross-ply laminate with side-to-thickness ratio $a/h = 10$. Transverse shear stresses computed through the thickness of the laminate τ_{yz} without spurious terms

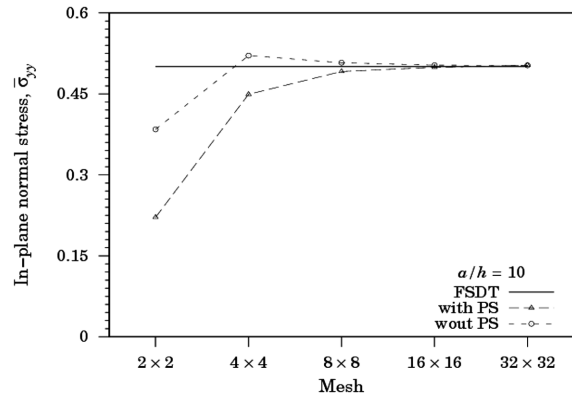
analytical solutions with mesh refinement. Table 1 shows that percent errors in σ_{xx} range from 61.85% to 0.04%, and percent errors in σ_{yy} range from 55.77% to 0.31% when the spurious terms are present. After elimination of the spurious terms, the percent errors in σ_{xx} range from 39.78% to 0.26%, and in σ_{yy} the percent errors range from 23.24% to 0.50%.

Further, Fig. 2(e) and Fig. 2(f) show the τ_{xz} solutions with and without the spurious terms, respectively, while Fig. 2(g) and Fig. 2(h) show the τ_{yz} solutions with and without the spurious terms, respectively. Again, the effects of the spurious terms are more pronounced in the coarse mesh solutions, being quite evident in the 2×2 mesh solutions. Table 1 shows that the percent errors are 85.61% and 155.70% in the coarser mesh solutions with the spurious terms for τ_{xz} and τ_{yz} , respectively. After elimination of the spurious terms, these percent errors fall to 40.03% and



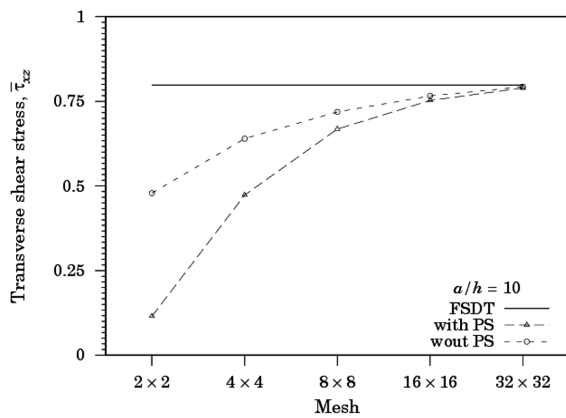
(i)

Fig. 2(i) Symmetric cross-ply laminate with side-to-thickness ratio $a/h = 10$. Convergence of normal stresses σ_{xx} solutions with and without parasitic shear



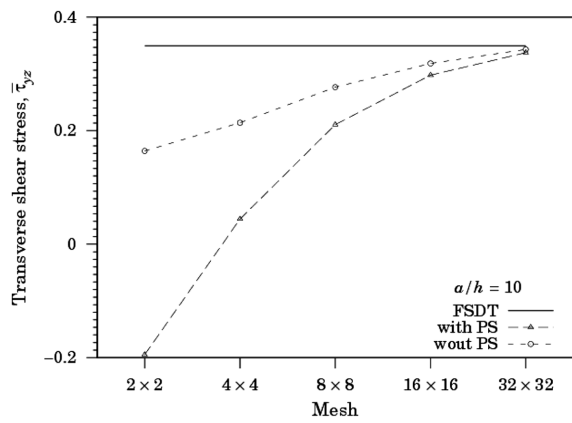
(j)

Fig. 2(j) Symmetric cross-ply laminate with side-to-thickness ratio $a/h = 10$. Convergence of normal stresses σ_{yy} solutions with and without parasitic shear



(k)

Fig. 2(k) Symmetric cross-ply laminate with side-to-thickness ratio $a/h = 10$. Convergence of transverse shear stresses τ_{xz} solutions with and without parasitic shear



(l)

Fig. 2(l) Symmetric cross-ply laminate with side-to-thickness ratio $a/h = 10$. Convergence of transverse shear stresses τ_{yz} solutions with and without parasitic shear

53.02%, respectively. All four models converge to the analytical solutions with mesh refinement, being the solutions provided by the models without the spurious terms slightly better. Percent errors for the corrected models are 0.63% and 1.88% for τ_{xz} and τ_{yz} , respectively.

Finally, Fig. 2(i) through Fig. 2(l) present convergence plots of the in-plane normal stresses and transverse shear stresses solutions, which aid in demonstrating their behaviors. The curves show that both solutions with and without the spurious terms converge to the analytical solution for all stresses. They also show the locking effect as the coarser meshes solutions provided by the model containing the spurious terms are always less accurate.

Next, solutions for the lower thickness plate ($a/h = 100$) are presented. Fig. 3(a) through Fig. 3(l)

Table 1 Percent errors in nondimensionalized stress components of symmetric cross-ply simply-supported square laminate ($0^\circ/90^\circ/90^\circ/0^\circ$)

$(0^\circ/90^\circ/90^\circ/0^\circ)$		Errors (%)							
		$\bar{\sigma}_{xx}$		$\bar{\sigma}_{yy}$		$\bar{\tau}_{yz}$		$\bar{\tau}_{xz}$	
a/h	Meshes	with/PS	wout/PS	with/PS	wout/PS	with/PS	wout/PS	with/PS	wout/PS
10	2×2	61.85	39.78	55.77	23.24	155.70	53.02	85.61	40.03
	4×4	18.63	6.80	10.25	4.08	87.36	38.81	40.72	19.83
	8×8	4.97	1.52	1.79	1.45	39.79	20.92	16.26	9.93
	16×16	1.16	0.27	0.25	0.51	14.82	8.93	5.72	4.02
	32×32	0.04	0.26	0.31	0.50	3.51	1.88	1.07	0.63
100	2×2	98.84	27.92	98.65	27.92	300.94	63.50	173.55	37.20
	4×4	93.20	5.67	92.10	7.17	355.30	44.26	189.54	17.63
	8×8	76.45	1.24	72.98	2.06	342.71	23.79	167.42	9.25
	16×16	44.22	0.20	38.06	0.63	243.00	10.16	99.48	3.76
	32×32	16.03	0.28	11.18	0.52	115.12	2.25	36.56	0.56

show the results of these analyses. In general, the results depicted by these figures show that the model containing the spurious terms presents poor convergence rates whereas the model without the spurious terms converges rather quickly. Fig. 3(a) and Fig. 3(c) show that the spurious terms delay convergence of the normal stresses σ_{xx} and σ_{yy} , and that even the finer meshes (32×32) present results which are far away from the analytical ones. Table 1 shows that percent errors in σ_{xx} range from 98.84% to 16.03%, and percent errors in σ_{yy} range from 98.65% to 11.18%. On the other hand, Fig. 3(b) and Fig. 3(d) show that when the spurious terms have been removed coarser meshes (8×8 , for instance) already present acceptable results (errors equal to 1.24% and 2.06%, respectively), and that the finer meshes (32×32) provides solutions which agree well with the analytical solutions (errors equal to 0.28% and 0.52%, respectively).

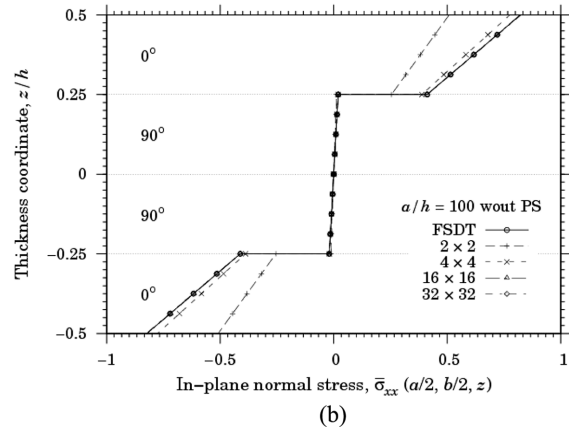
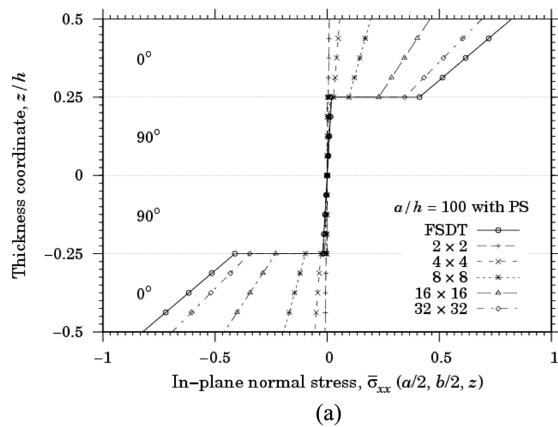
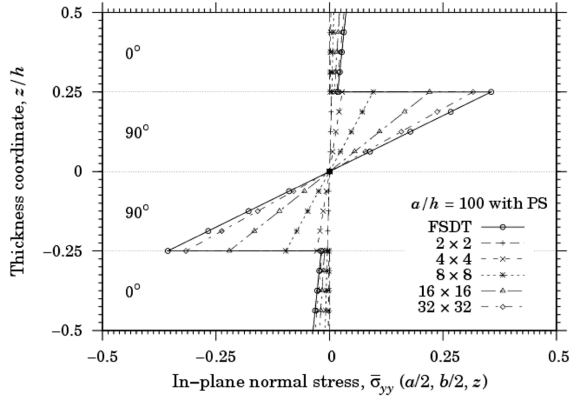


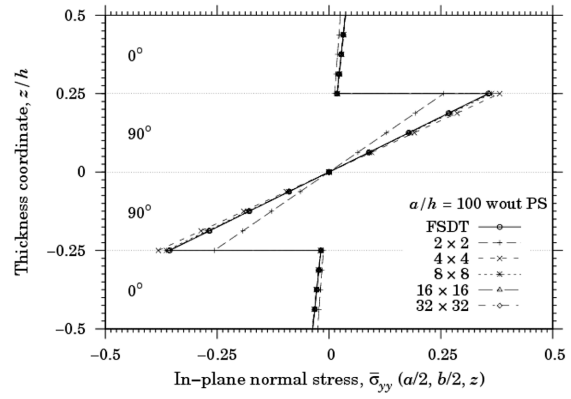
Fig. 3(a) Symmetric cross-ply laminate with side-to-thickness ratio $a/h = 100$. Normal stresses σ_{xx} computed through the thickness of the laminate with spurious terms

Fig. 3(b) Symmetric cross-ply laminate with side-to-thickness ratio $a/h = 100$. Normal stresses σ_{xx} computed through the thickness of the laminate without spurious terms



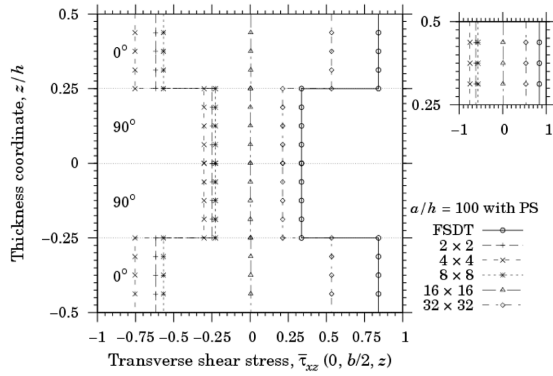
(c)

Fig. 3(c) Symmetric cross-ply laminate with side-to-thickness ratio $a/h = 100$. Normal stresses σ_{yy} computed through the thickness of the laminate with spurious terms



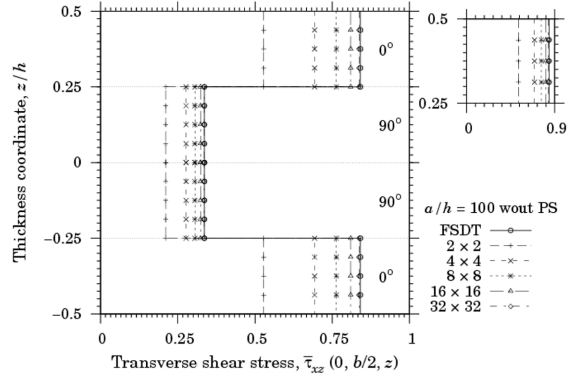
(d)

Fig. 3(d) Symmetric cross-ply laminate with side-to-thickness ratio $a/h = 100$. Normal stresses σ_{yy} computed through the thickness of the laminate without spurious terms



(e)

Fig. 3(e) Symmetric cross-ply laminate with side-to-thickness ratio $a/h = 100$. Transverse shear stresses τ_{xz} computed through the thickness of the laminate with spurious terms



(f)

Fig. 3(f) Symmetric cross-ply laminate with side-to-thickness ratio $a/h = 100$. Transverse shear stresses τ_{xz} computed through the thickness of the laminate without spurious terms

Fig. 3(e) through Fig. 3(h) show the solutions for the transverse shear stresses τ_{xz} and τ_{yz} . Fig. 3(e) and Fig. 3(g) contain the solutions when the spurious terms are present in the model. Observing those plots, it is seen that the solutions provided by coarser meshes diverge from the FSDT solutions, leading to completely erroneous results. Only the solution of the finer mesh (32×32) approaches the analytical solution throughout the thickness of the laminate. Table 1 shows that the smallest percent errors are 36.56% and 115.12%, respectively. The enlarged details of the plots allow for the reader to see more easily the convergence delays caused by the spurious (parasitic shear) terms. Fig. 3(f) and Fig. 3(h) show the solutions for τ_{xz} and τ_{yz} computed after the spurious terms have been removed. It can be seen that those solutions converge well within the analytical ones. The enlarged details of the plots help to demonstrate that there is very good agreement

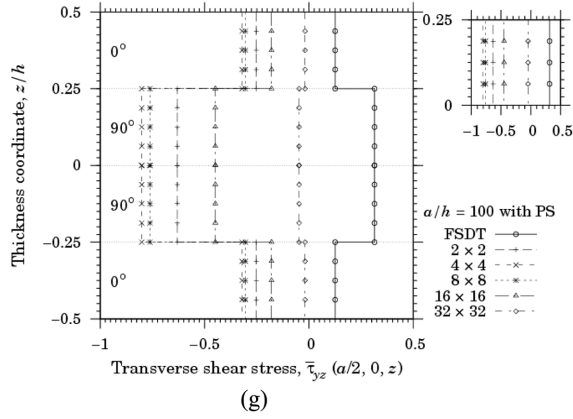


Fig. 3(g) Symmetric cross-ply laminate with side-to-thickness ratio $a/h = 100$. Transverse shear stresses τ_{yz} computed through the thickness of the laminate with spurious terms

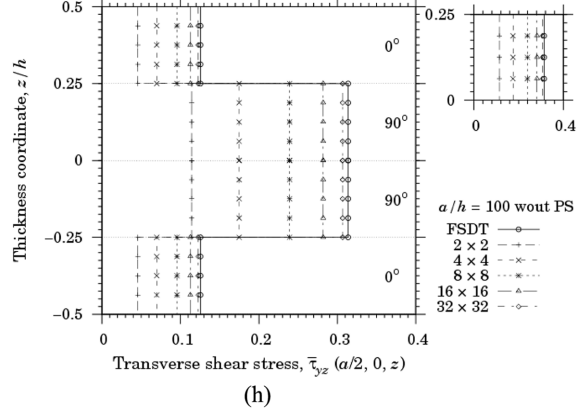


Fig. 3(h) Symmetric cross-ply laminate with side-to-thickness ratio $a/h = 100$. Transverse shear stresses computed through the thickness of the laminate τ_{yz} without spurious terms

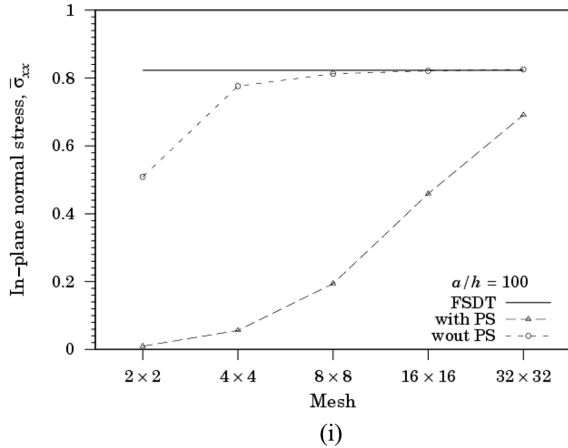


Fig. 3(i) Symmetric cross-ply laminate with side-to-thickness ratio $a/h = 100$. Convergence of normal stresses σ_{xx} solutions with and without parasitic shear

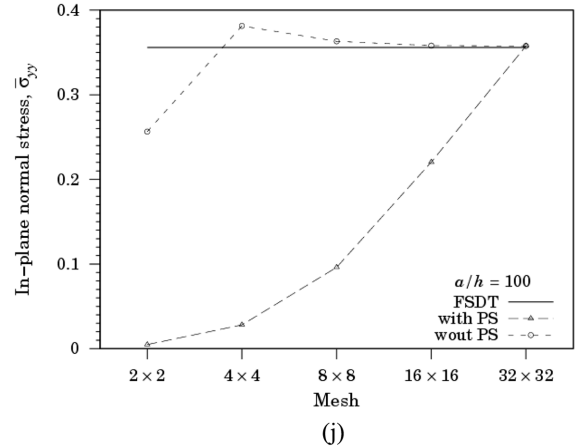


Fig. 3(j) Symmetric cross-ply laminate with side-to-thickness ratio $a/h = 100$. Convergence of normal stresses σ_{yy} solutions with and without parasitic shear

between the 32×32 meshes solutions and the analytical solutions. For these meshes, the largest percent errors are 0.56% and 2.25%, respectively.

Fig. 3(i) through Fig. 3(l) present convergence plots of the normal stresses and transverse shear stresses solutions, which aid in demonstrating their behaviors. The reader can observe that the solutions without the spurious terms approach the analytical solutions asymptotically with mesh refinement for both normal and transverse shear stresses. Fig. 3(i) and Fig. 3(j) also show that the solutions for the normal stresses σ_{xx} and σ_{yy} containing the spurious terms tend to converge to the analytical solutions slowly, indicating that more computational effort would be required. Further, Fig. 3(k) and Fig. 3(l) show that the solutions for transverse shear stresses containing the spurious terms tend to converge, however very slowly and not monotonically.

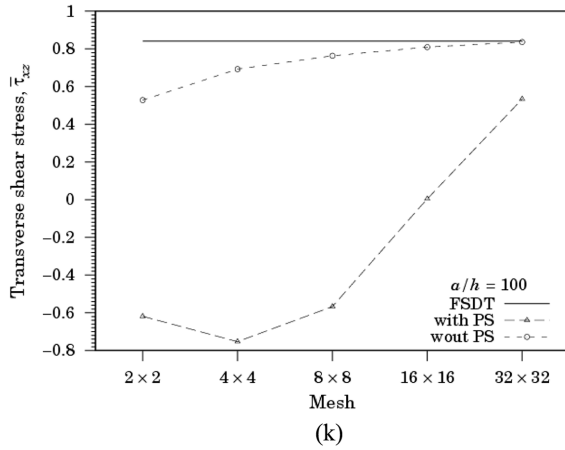


Fig. 3(k) Symmetric cross-ply laminate with side-to-thickness ratio $a/h = 100$. Convergence of transverse shear stresses τ_{xz} solutions with and without parasitic shear

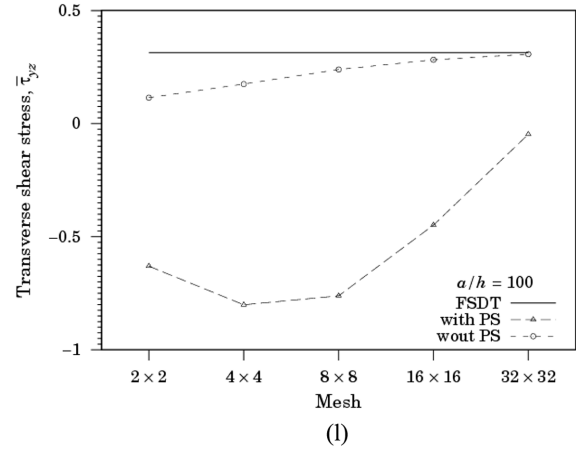


Fig. 3(l) Symmetric cross-ply laminate with side-to-thickness ratio $a/h = 100$. Convergence of transverse shear stresses τ_{yz} solutions with and without parasitic shear

4.2 Problem #2

The second problem is an angle-ply antisymmetric laminate with lamination scheme $-45^\circ/+45^\circ$. The plate is square ($a = b = 1.0$ m) and simply supported, and it is subjected to a sinusoidal load given by the following expression

$$q(x, y) = q_o \sin \frac{\pi x}{a} \sin \frac{\pi y}{b} \tag{59}$$

where $q_o = 10$ N/m². The plate is solved both with side-to-thickness ratios $a/h = 10$ and $a/h = 100$. In-plane normal stresses σ_{xx} are calculated at the center point of the plate, while transverse shear

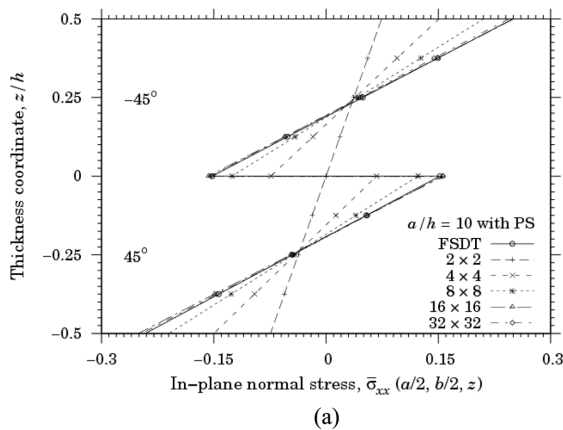


Fig. 4(a) Anti-Symmetric angle-ply laminate with side-to-thickness ratio $a/h = 10$. Normal stresses σ_{xx} computed through the thickness of the laminate with spurious terms.

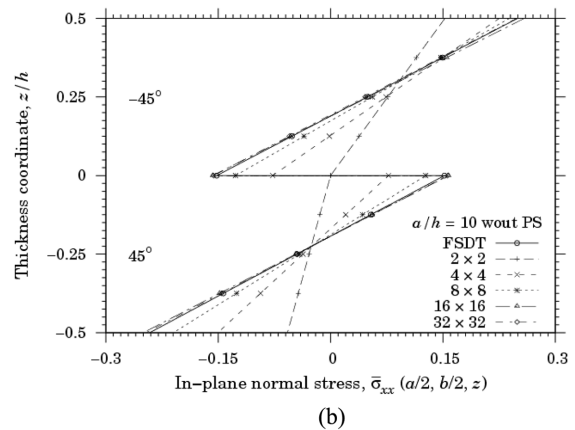


Fig. 4(b) Anti-Symmetric angle-ply laminate with side-to-thickness ratio $a/h = 10$. Normal stresses σ_{xx} computed through the thickness of the laminate without spurious terms

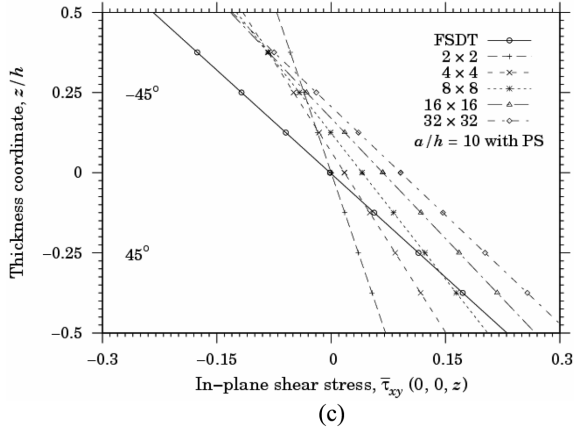


Fig. 4(c) Anti-Symmetric angle-ply laminate with side-to-thickness ratio $a/h = 10$. In-plane shear stresses τ_{xy} computed through the thickness of the laminate with spurious terms

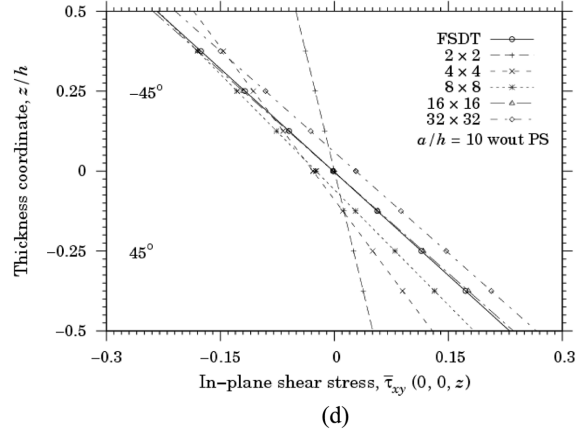


Fig. 4(d) Anti-Symmetric angle-ply laminate with side-to-thickness ratio $a/h = 10$. In-plane shear stresses τ_{xy} computed through the thickness of the laminate without spurious terms

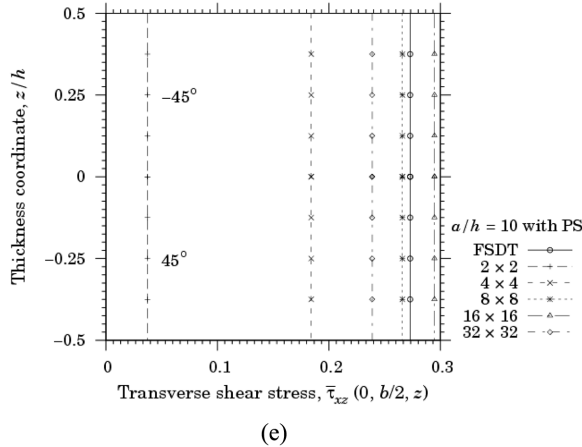


Fig. 4(e) Anti-Symmetric angle-ply laminate with side-to-thickness ratio $a/h = 10$. Transverse shear stresses τ_{xz} computed through the thickness of the laminate with spurious terms

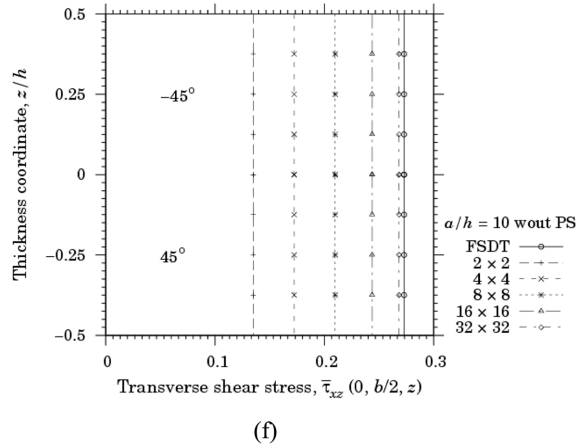
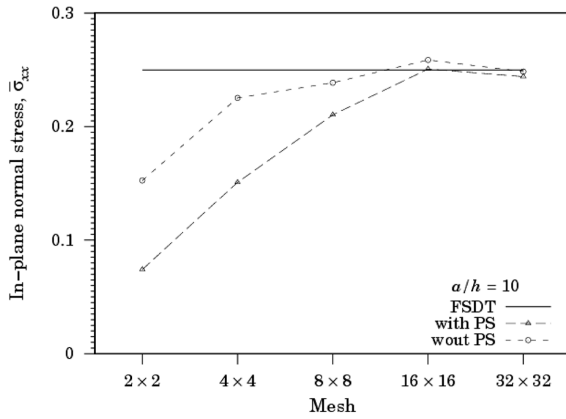


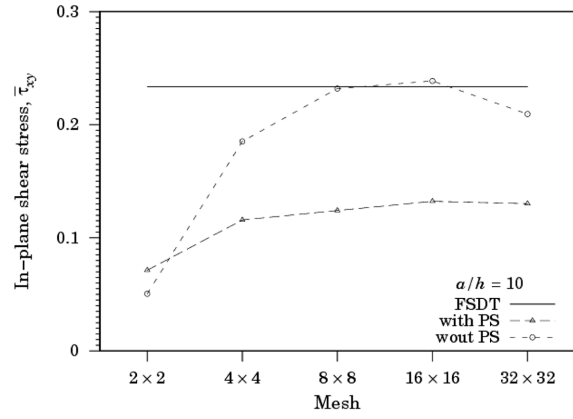
Fig. 4(f) Anti-Symmetric angle-ply laminate with side-to-thickness ratio $a/h = 10$. Transverse shear stresses τ_{xz} computed through the thickness of the laminate without spurious terms

stresses τ_{xz} are calculated at the middle point of the xz -plane border, and the in-plane shear stresses τ_{xy} are calculated at a corner point.

First, solutions for the higher thickness plate ($a/h = 10$) are presented. Fig. 4(a) through Fig. 4(i) show the results of these analyses. Fig. 4(a) and Fig. 4(b) depict the results of the normal stresses σ_{xx} through the thickness of the laminate for the models with and without the spurious terms, respectively. It can be seen that effects of spurious terms are apparent only in the coarse model solution, and that both models converge to the analytical solution. Table 2 shows that percent errors in σ_{xx} range from 70.31% to 2.30% when the spurious terms are present. After elimination of the



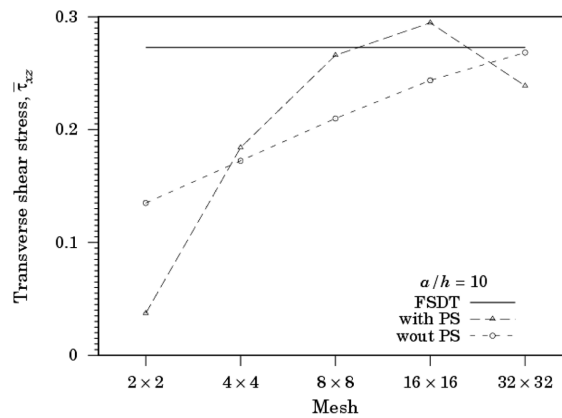
(g)



(h)

Fig. 4(g) Anti-Symmetric angle-ply laminate with side-to-thickness ratio $a/h = 10$. Convergence of normal stresses σ_{xx} solutions with and without parasitic shear

Fig. 4(h) Anti-Symmetric angle-ply laminate with side-to-thickness ratio $a/h = 10$. Convergence of in-plane shear stresses τ_{xy} solutions with and without parasitic shear



(i)

Fig. 4(i) Anti-Symmetric angle-ply laminate with side-to-thickness ratio $a/h = 10$. Convergence of transverse shear stresses τ_{xz} solutions with and without parasitic shear.

spurious terms, the percent errors in σ_{xx} range from 38.89% to 0.53%. Fig. 4(c) and Fig. 4(d) show the results of the in-plane shear stress τ_{xy} through the thickness of the laminate for the models with and without the spurious terms, respectively. Here effects of spurious terms are significant. The plots show that the numerical solution gets farther away from the analytical solution with mesh refinement. Percent errors results displayed in Table 2, although they decrease slightly with refinement, are very high. Their values range between 69.45% and 44.28%. On the other hand, solutions provided by the model without the spurious terms converge to the analytical one with mesh refinement as depicted by the plots in Fig. 4(d). It is observed, however, that the best solution is provided by the second finer mesh (16×16), and that the finer mesh (32×32) solution actually diverges from the analytical solution. The percent errors range from 78.36% to only 2.17% when

Table 2 Percent errors in nondimensionalized stress components of anti-symmetric angle-ply simply-supported square laminate ($-45^\circ/+45^\circ$)

$(-45^\circ/+45^\circ)$		Errors (%)					
		$\bar{\sigma}_{xx}$		$\bar{\tau}_{xz}$		$\bar{\tau}_{xy}$	
a/h	Meshes	with/PS	wout/PS	with/PS	wout/PS	with/PS	wout/PS
10	2×2	70.31	38.89	86.33	50.51	69.45	78.36
	4×4	39.57	9.83	32.50	36.81	50.44	20.72
	8×8	15.77	4.45	2.56	23.07	46.86	0.70
	16×16	0.36	3.56	8.01	10.67	43.40	2.17
	32×32	2.30	0.53	12.49	1.66	44.28	10.36
100	2×2	98.81	38.89	194.45	50.51	98.77	78.36
	4×4	95.16	6.96	195.97	30.02	94.36	23.69
	8×8	82.23	5.28	117.67	20.67	81.55	12.01
	16×16	52.49	2.84	196.62	5.97	62.89	18.10
	32×32	25.86	1.16	500.51	5.14	58.62	34.47

the model is refined up to the 16×16 mesh, showing that good results are obtained. However, the finer mesh (32×32) is associated to an error of 10.36%.

Further, Fig. 4(e) and Fig. 4(f) depict the solutions of transverse shear stress τ_{xz} with and without the spurious terms, respectively. Effects of spurious terms can be noticed in the solutions of Fig. 4(e). Although the 8×8 mesh solution approaches the analytical solution, further refinement provides poorer solutions. The percent errors for the first three meshes range from 86.33% to 2.56%, but they increase to 8.01% and to 12.49%, respectively, in the further refinements. After elimination of the spurious terms, solutions improve and present monotonic convergence towards the analytical solution as shown in Fig. 4(f), and in Table 2 where the percent errors range from 50.51% to only 1.66%. Finally, convergence plots for solutions with and without the spurious terms are presented in Fig. 4(g) through Fig. 4(i). These plots reinforce the stresses behaviors described above. In general, solutions without the spurious terms converge to the analytical solution and present good accuracy. The locking effect in the solutions with the spurious terms is emphasized by the plots, being more pronounced in the shear stresses solutions. That is, the spurious terms prevent the shear stresses solutions to converge to the analytical solutions. Further, as already noted above, the corrected solution for the in-plane shear stress τ_{xy} does not present monotonic convergence either. The corresponding convergence plot (Fig. 4(h)) shows that the result from the 32×32 mesh analysis deviates significantly from the analytical solution value.

Next, solutions for the lower thickness plate ($a/h = 100$) are presented. Fig. 5(a) through Fig. 5(i) show the results of these analyses. Fig. 5(a) and Fig. 5(b) depict the results of the normal stresses σ_{xx} through the thickness of the laminate for the models with and without the spurious terms, respectively. Solution provided by the corrected model converges well to the analytical solution. Although refinement attenuates locking and the solution of the model containing the spurious terms tends to converge to the analytical solution, accuracy provided by its finer mesh is not acceptable for most points. Table 2 shows that the percent errors for the model containing the spurious terms range from 98.81% to 25.86%, whereas the percent errors for the corrected model range from 38.89% to only 1.16%.

Fig. 5(c) and Fig. 5(d) show the results of the in-plane shear stresses τ_{xy} through the thickness of

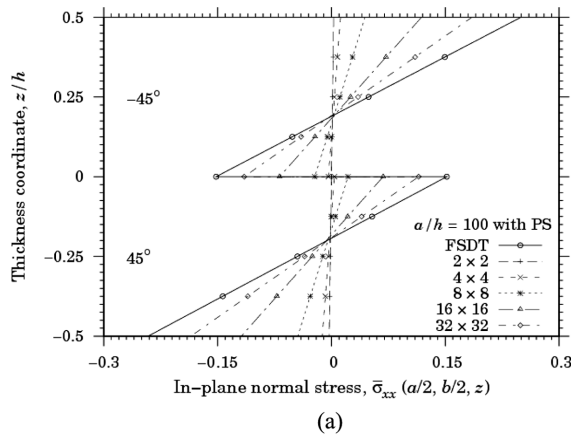


Fig. 5(a) Anti-Symmetric angle-ply laminate with side-to-thickness ratio $a/h = 100$. Normal stresses σ_{xx} computed through the thickness of the laminate with spurious terms

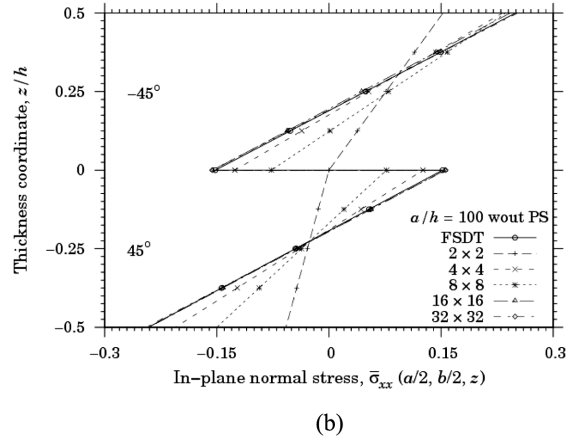


Fig. 5(b) Anti-Symmetric angle-ply laminate with side-to-thickness ratio $a/h = 100$. Normal stresses σ_{xx} computed through the thickness of the laminate without spurious terms

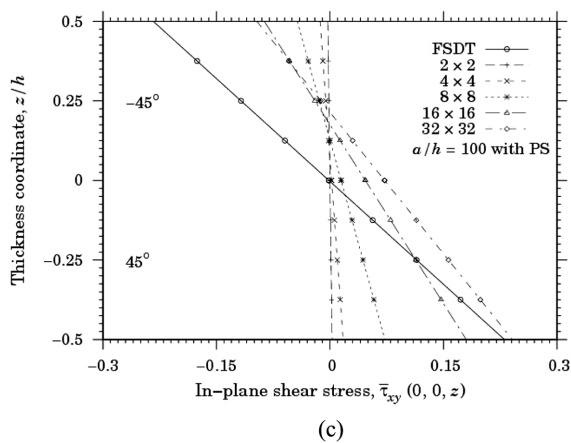


Fig. 5(c) Anti-Symmetric angle-ply laminate with side-to-thickness ratio $a/h = 100$. In-plane shear stresses τ_{xy} computed through the thickness of the laminate with spurious terms

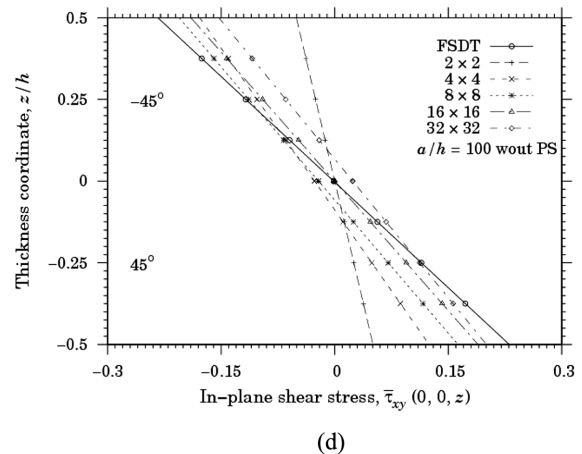


Fig. 5(d) Anti-Symmetric angle-ply laminate with side-to-thickness ratio $a/h = 100$. In-plane shear stresses τ_{xy} computed through the thickness of the laminate without spurious terms

the laminate for the models with and without the spurious terms, respectively. The model with the spurious terms provides solutions which do not converge to the analytical solution. The percent errors in Table 2 range from 98.77% to 58.62%, which are unacceptable. Solutions provided by the model without the spurious terms are better, although results do not present monotonic convergence. Examining Fig. 5(d) closely, it is seen that results provided by the coarser meshes approach the analytical solution better than the results provided by the finer meshes at some points in the top lamina, which is unexpected. In the bottom lamina, however, the best results correspond to the finer meshes although the 16×16 mesh provides better results than the 32×32 mesh at the points closer

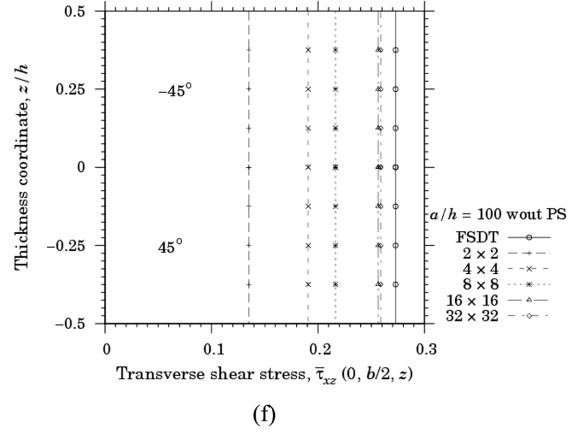
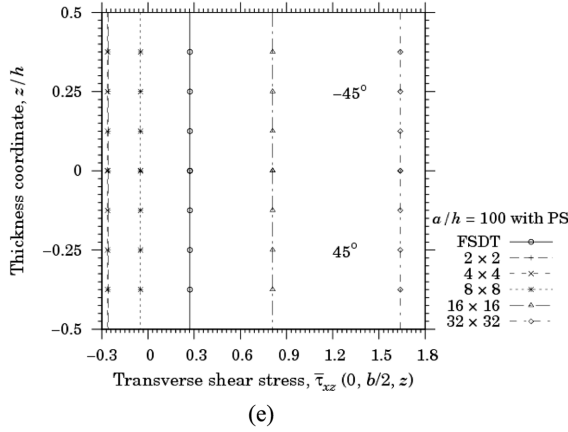


Fig. 5(e) Anti-Symmetric angle-ply laminate with side-to-thickness ratio $a/h = 100$. Transverse shear stresses τ_{xz} computed through the thickness of the laminate with spurious terms

Fig. 5(f) Anti-Symmetric angle-ply laminate with side-to-thickness ratio $a/h = 100$. Transverse shear stresses τ_{xz} computed through the thickness of the laminate without spurious terms

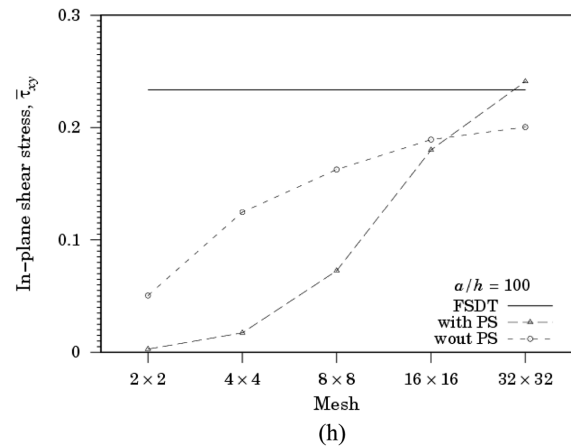
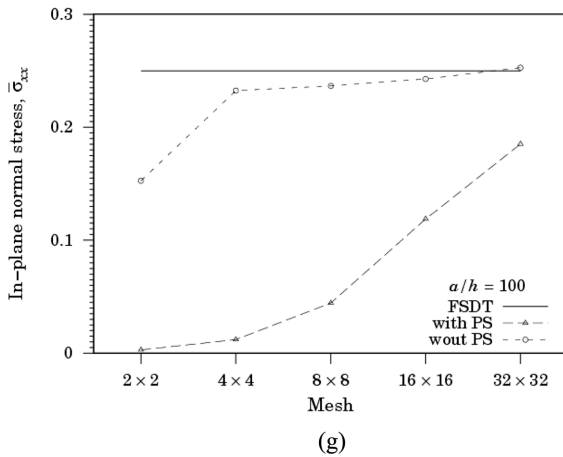


Fig. 5(g) Anti-Symmetric angle-ply laminate with side-to-thickness ratio $a/h = 100$. Convergence of normal stresses σ_{xx} solutions with and without parasitic shear

Fig. 5(h) Anti-Symmetric angle-ply laminate with side-to-thickness ratio $a/h = 100$. Convergence of in-plane shear stresses τ_{xy} solutions with and without parasitic shear

to the middle surface. The percent errors shown in Table 2 correspond to stress values in the top lamina. The errors associated to the first three meshes decrease from 78.36% to 12.01%, but they increase to 18.10% and to 34.47%, respectively, in the further refinements.

Further, Fig. 5(e) and Fig. 5(f) depict the solutions of transverse shear stresses τ_{xz} with and without the spurious terms, respectively. Effects of spurious terms are significant in these solutions. Coarse meshes solutions are much smaller than the analytical one whereas further refinement provides solutions that greatly diverge from the analytical solution. As shown in Table 2, the percent error corresponding to the coarser mesh is 194.45% whereas its value for the finer mesh is

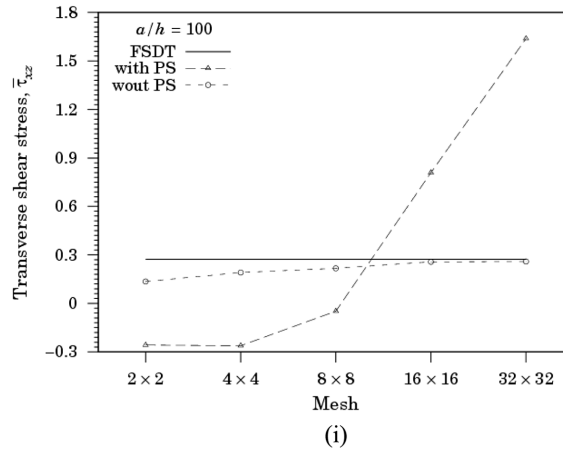


Fig. 5(i) Anti-Symmetric angle-ply laminate with side-to-thickness ratio $a/h = 100$. Convergence of transverse shear stresses τ_{xz} solutions with and without parasitic shear

500.51%. However, solutions provided by the model corrected for the spurious terms present monotonic convergence and good accuracy when compared to the analytical solution, as shown in Fig. 5(f). Percent errors in Table 2 range from 50.51% to 5.14%. Finally, convergence plots for solutions with and without the spurious terms are presented in Fig. 5(g) through Fig. 5(i). The reader can observe that the solutions without the spurious terms approach the analytical solutions gradually with mesh refinement for both normal and transverse shear stresses. Fig. 5(g) also shows that the spurious terms lock the model such that convergence of σ_{xx} appears to occur, but very slowly. Fig. 5(h) and Fig. 5(i), however, show that the spurious terms do not allow shear stresses to converge. The erratic behavior of the transverse shear stresses is emphasized.

4.3 Problem #3

The third problem is a square non-symmetric cross-ply laminated composite plate with two opposite edges simply supported and the other two opposite edges free subjected to a sinusoidal load defined by Eq. (59). The laminate is composed of two laminae with lamination scheme $0^\circ/90^\circ$, and the sides of the laminate are 1.0 m in length ($a = b = 1.0$ m). The plate is solved both with

Table 3 Percent errors in nondimensionalized stress components of non-symmetric cross-ply square laminate ($0^\circ/90^\circ$) with two opposite free edges and two opposite simply supported edges

(0°/90°)		Errors (%)					
a/h	Meshes	$\bar{\sigma}_{xx}$		$\bar{\sigma}_{yy}$		$\bar{\tau}_{yz}$	
		with/PS	wout/PS	with/PS	wout/PS	with/PS	wout/PS
10	2 × 2	24.78	50.06	67.03	45.59	109.23	19.33
	4 × 4	8.06	15.93	39.45	24.93	12.83	13.51
	8 × 8	4.87	11.78	10.38	4.75	22.40	2.64
	16 × 16	1.15	2.77	3.40	1.84	18.87	1.85
	32 × 32	1.14	0.79	1.06	0.64	11.14	1.28

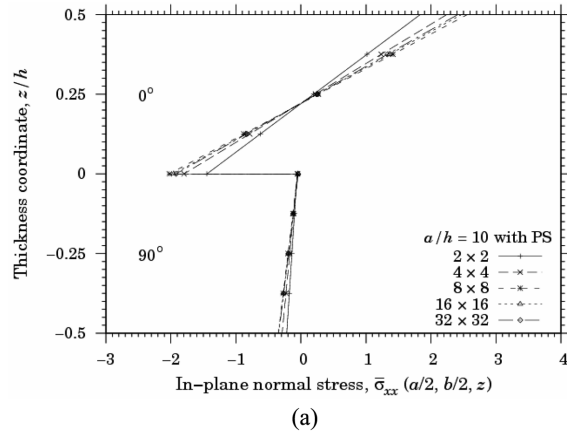


Fig. 6(a) Non-Symmetric cross-ply laminate with side-to-thickness ratio $a/h = 10$. Normal stresses σ_{xx} computed through the thickness of the laminate with spurious terms

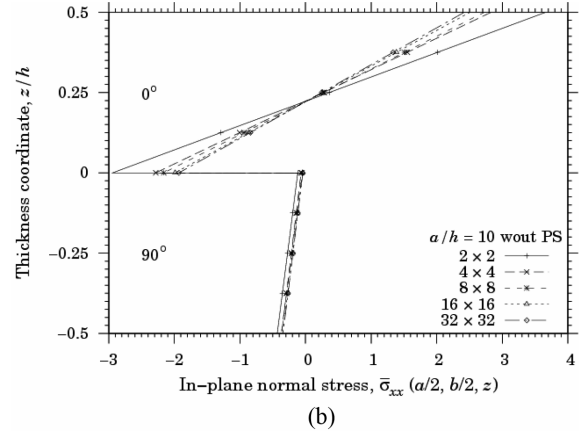


Fig. 6(b) Non-Symmetric cross-ply laminate with side-to-thickness ratio $a/h = 10$. Normal stresses σ_{xx} computed through the thickness of the laminate without spurious terms

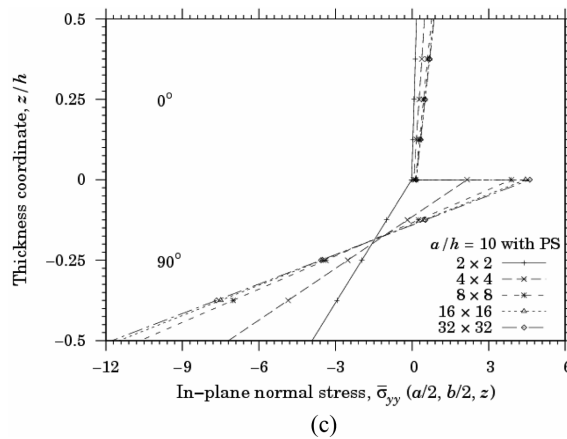


Fig. 6(c) Non-Symmetric cross-ply laminate with side-to-thickness ratio $a/h = 10$. Normal stresses σ_{yy} computed through the thickness of the laminate with spurious terms

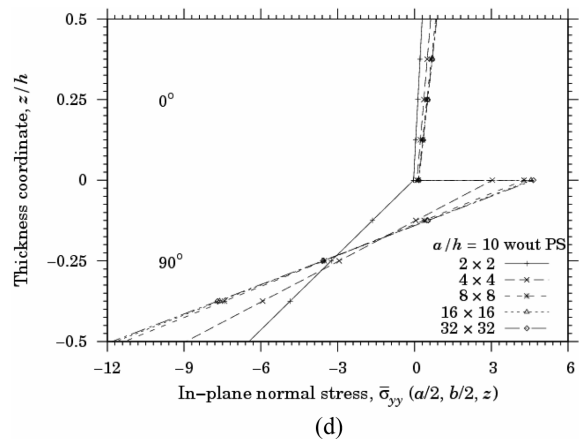


Fig. 6(d) Non-Symmetric cross-ply laminate with side-to-thickness ratio $a/h = 10$. Normal stresses σ_{yy} computed through the thickness of the laminate without spurious terms

side-to-thickness ratios $a/h = 10$ and $a/h = 100$. In-plane normal stresses σ_{xx} and σ_{yy} are calculated at the center point of the plate, while transverse shear stresses τ_{yz} are calculated at borders middle points. Analytical solutions are not available, except for the maximum stresses values for the case where $a/h = 10$ (Reddy 2004). Percent errors contained in Table 3 are referred to those maximum stresses values.

First, solutions for the higher thickness plate ($a/h = 10$) are presented. Fig. 6(a) through Fig. 6(i) show the results of these analyses. Fig. 6(a) and Fig. 6(b) show the σ_{xx} solutions with and without the spurious terms, respectively. According to the plots in Fig. 6(a), the spurious terms prevent convergence to be monotonic. This is easily seen at the middle surface and on the middle of the top

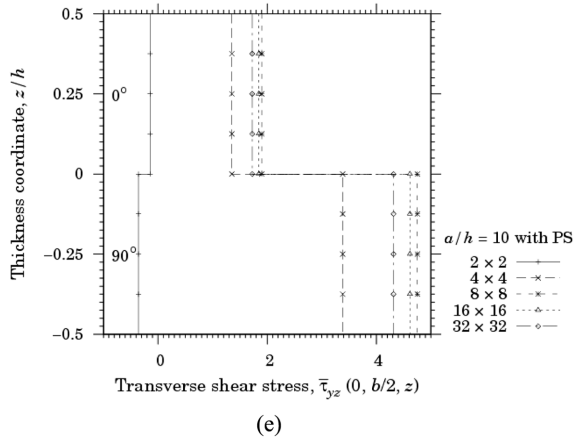


Fig. 6(e) Non-Symmetric cross-ply laminate with side-to-thickness ratio $a/h = 10$. Transverse shear stresses τ_{yz} computed through the thickness of the laminate with spurious terms

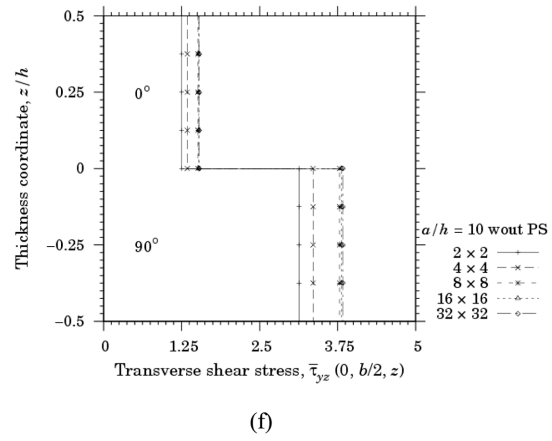


Fig. 6(f) Non-Symmetric cross-ply laminate with side-to-thickness ratio $a/h = 10$. Transverse shear stresses τ_{yz} computed through the thickness of the laminate without spurious terms

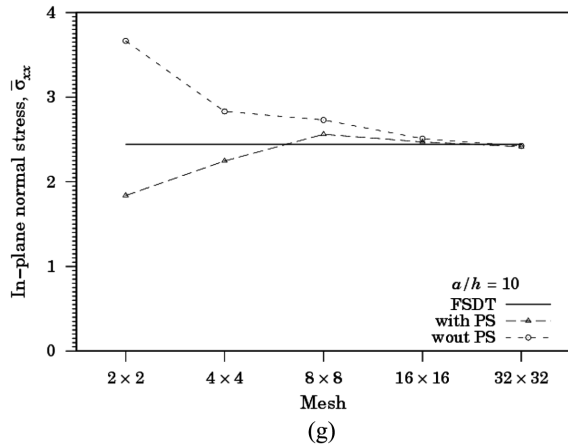


Fig. 6(g) Non-Symmetric cross-ply laminate with side-to-thickness ratio $a/h = 10$. Convergence of normal stresses σ_{xx} solutions with and without parasitic shear.

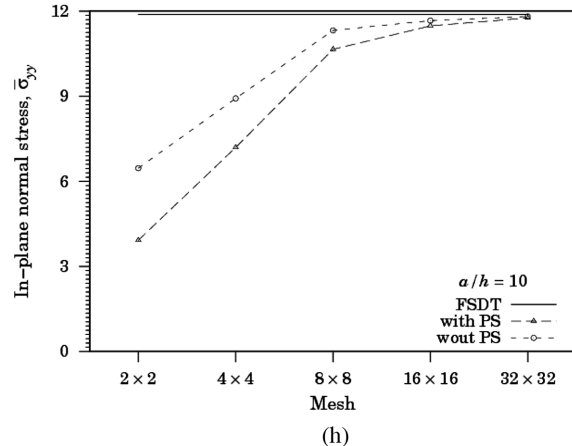


Fig. 6(h) Non-Symmetric cross-ply laminate with side-to-thickness ratio $a/h = 10$. Convergence of normal stresses σ_{yy} solutions with and without parasitic shear

lamina where the values provided by the 32×32 mesh are not the extreme ones. This erroneous behavior is corrected by the removal of the spurious terms as shown by Fig. 6(b). It can be seen that convergence is monotonic as the solution provided by the 32×32 mesh contains the extreme values. Table 3 shows that percent errors are larger in the corrected model, except in the last solution (32×32 mesh). These error values range from 50.06% to 0.79%. Percent errors in the model containing the spurious terms range from 24.78% to 1.14%.

Fig. 6(c) and Fig. 6(d) show the σ_{yy} solutions with and without the spurious terms, respectively. The plots show that the spurious terms have a more significant effect on the coarse meshes

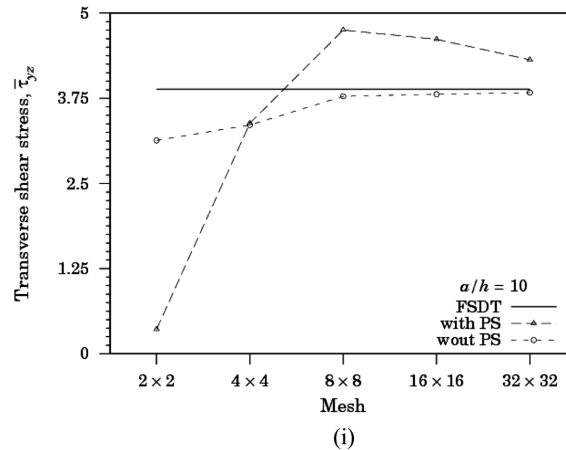


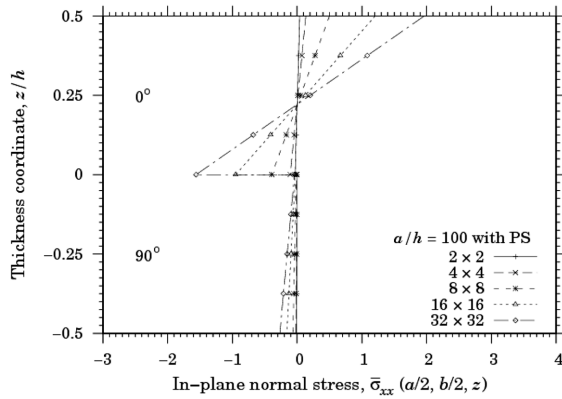
Fig. 6(i) Non-Symmetric cross-ply laminate with side-to-thickness ratio $a/h = 10$. Convergence of transverse shear stresses τ_{yz} solutions with and without parasitic shear

solutions. As refinement is proceeded on, the locking effect is attenuated. Both models converge to the same solution, maintaining a small numerical difference between their final solutions. Table 3 shows that the percent errors of the model containing the spurious terms range from 67.03% to 1.06%, while the percent errors of the corrected model range from 45.59% to 0.64%.

Further, Fig. 6(e) and Fig. 6(f) show the τ_{yz} solutions with and without the spurious terms, respectively. It is seen that the spurious terms prevent convergence of the transverse shear stresses to occur. Results are oscillatory as values provided by the 8×8 mesh are higher than the ones provided by the 16×16 mesh, which in turn are higher than the ones provided by the 32×32 mesh. Removal of the spurious terms corrects this behavior. Fig. 6(f) shows monotonic convergence of transverse shear stresses.

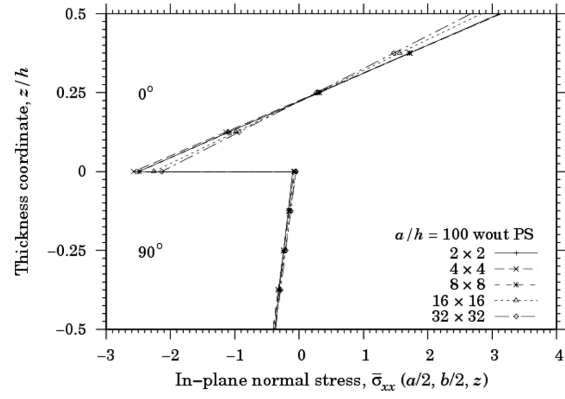
Finally, Fig. 6(g) through Fig. 6(i) present convergence plots of the normal stresses and transverse shear stresses solutions, which aid in demonstrating their behaviors. Fig. 6(g) shows that both models converge to the analytical solution value of σ_{xx} . Convergence of the corrected model occurs from above, while the values of the model containing the spurious terms oscillates around the analytical solution value. These plots also clearly demonstrate that errors in the corrected model are initially larger, and that are only considerably reduced in the last solution. Fig. 6(h) show that both models provide convergent solutions to σ_{yy} . Locking is significant in the coarse meshes, being attenuated with refinement. Fig. 6(i) shows the strong effect of the spurious terms on the solution of τ_{yz} . The corrected model converges monotonically to the analytical solution.

Next, solutions for the lower thickness plate ($a/h = 100$) are presented. Fig. 7(a) through Fig. 7(i) show the results of these analyses. In general, the results depicted by these figures show that the model containing the spurious terms presents poor convergence rates whereas the model without the spurious terms converges rather quickly. In the absence of an analytical solution, percent errors have not been produced. Fig. 7(a) and Fig. 7(b) show the σ_{xx} solutions with and without the spurious terms, respectively. It can be seen that the locking effect caused by the spurious terms are very significant even for the last refinement. Results are severely underestimated by the model containing the spurious terms. Further it is shown by Fig. 7(b) that convergence of the solution provided by the corrected model occurs from above.



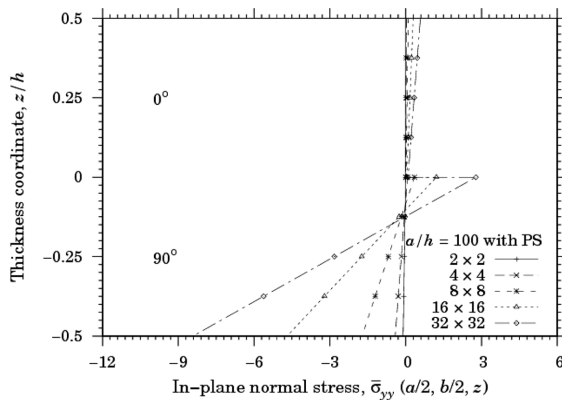
(a)

Fig. 7(a) Non-Symmetric cross-ply laminate with side-to-thickness ratio $a/h = 100$. Normal stresses σ_{xx} computed through the thickness of the laminate with spurious terms.



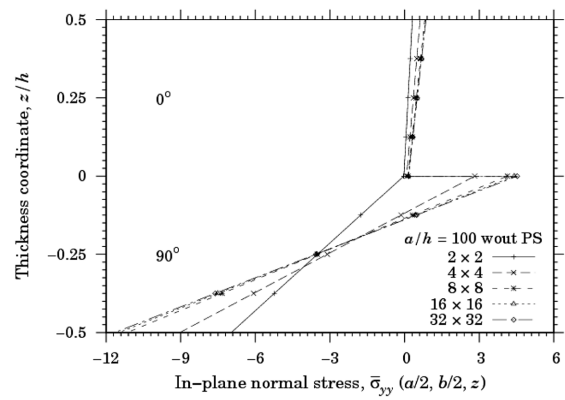
(b)

Fig. 7(b) Non-Symmetric cross-ply laminate with side-to-thickness ratio $a/h = 100$. Normal stresses σ_{xx} computed through the thickness of the laminate without spurious terms



(c)

Fig. 7(c) Non-Symmetric cross-ply laminate with side-to-thickness ratio $a/h = 100$. Normal stresses σ_{yy} computed through the thickness of the laminate with spurious terms



(d)

Fig. 7(d) Non-Symmetric cross-ply laminate with side-to-thickness ratio $a/h = 100$. Normal stresses σ_{yy} computed through the thickness of the laminate without spurious terms

Fig. 7(c) and Fig. 7(d) show the σ_{yy} solutions with and without the spurious terms, respectively. Again, the locking effect is very significant, causing the results to be underestimated. Similar observations can be made regarding the τ_{yz} solutions with and without the spurious terms depicted in Fig. 7(e) and Fig. 7(f), respectively. The spurious terms prevent convergence. The coarse meshes provide solutions which are very different than the solutions provided by the finer meshes. Solutions provided by the model corrected for the spurious terms seem to converge, although convergence is not monotonic as oscillations occur.

Finally, Fig. 7(g) through Fig. 7(i) present convergence plots of the normal stresses and transverse shear stresses solutions, which aid in interpreting their behaviors. Fig. 7(g) and Fig. 7(h) clearly

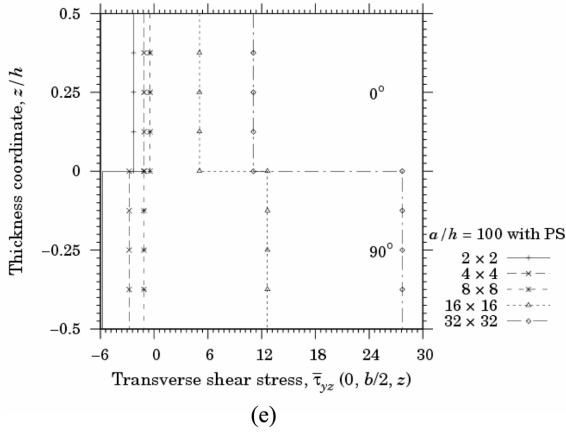


Fig. 7(e) Non-Symmetric cross-ply laminate with side-to-thickness ratio $a/h = 100$. Transverse shear stresses τ_{yz} computed through the thickness of the laminate with spurious terms

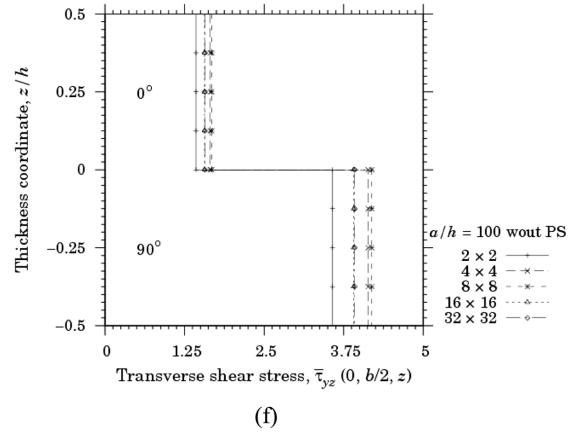


Fig. 7(f) Non-Symmetric cross-ply laminate with side-to-thickness ratio $a/h = 100$. Transverse shear stresses τ_{yz} computed through the thickness of the laminate without spurious terms

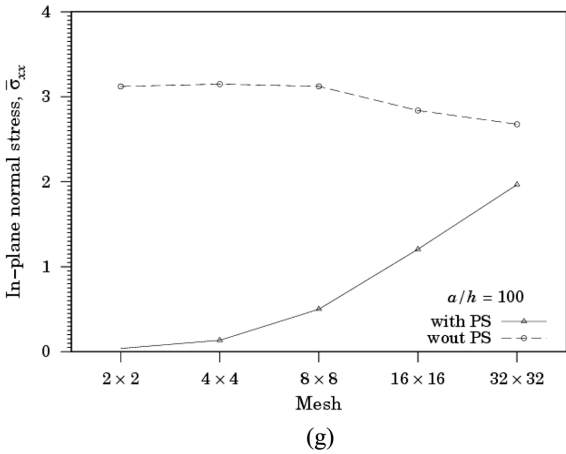


Fig. 7(g) Non-Symmetric cross-ply laminate with side-to-thickness ratio $a/h = 100$. Convergence of normal stresses σ_{xx} solutions with and without parasitic shear

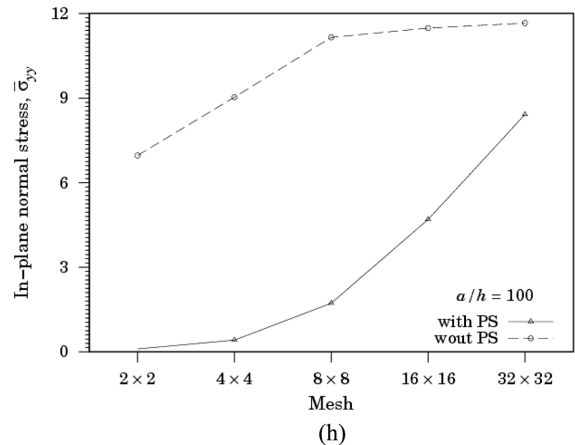


Fig. 7(h) Non-Symmetric cross-ply laminate with side-to-thickness ratio $a/h = 100$. Convergence of normal stresses σ_{yy} solutions with and without parasitic shear

show the locking caused by the spurious terms in the solutions of σ_{xx} and σ_{yy} . Fig. 7(i) shows that the solution for τ_{yz} provided by the corrected model change very little from mesh to mesh. Also, the coarser meshes solutions with the spurious terms are closer to the corrected solution than the ones provided by the finer meshes. Results of the latter are very much in error with respect to the solution provided by the corrected model.

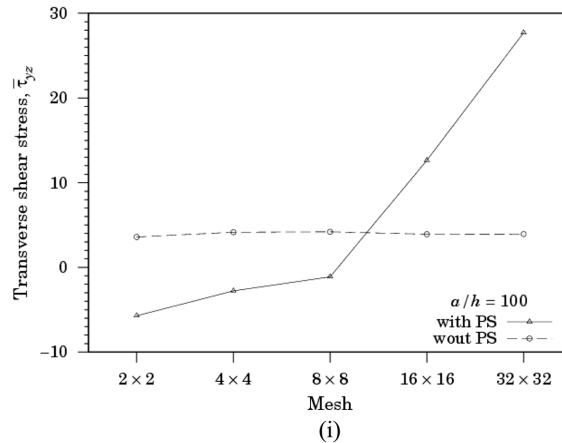


Fig. 7(i) Non-Symmetric cross-ply laminate with side-to-thickness ratio $a/h = 100$. Convergence of transverse shear stresses τ_{yz} solutions with and without parasitic shear

5. Conclusions

This work is concerned with the modeling of laminated composite plates employing the finite element method. It focuses on the locking of the bilinear plate element and how it affects numerical solutions. Further, it is concerned with identifying and eliminating the sources of locking employing a procedure which is alternative to classical ones (reduced-order integration, for instance).

A four-node plate element formulated using strain gradient notation has been presented. Strain gradient notation is a physically interpretable notation which allows for the *a-priori* determination of the element's modeling capabilities and deficiencies. The shear strain polynomial expansions of the element were inspected and showed to possess spurious terms. Specifically, those terms are first- and second-order normal strain terms, which do not contribute physically to the shear deformation of the plate. They cause shear locking by increasing the shear strain energy of the element unduly when activated during deformation. For this reason, these spurious terms are referred to as parasitic shear terms (Dow 1999). This terminology is employed in this paper. Using the transparency of the notation, the element was corrected by simply removing the parasitic shear terms from the shear strain expressions.

Higher thickness and lower thickness plates have been analyzed here for different lamination schemes, boundary and loading conditions. In each case, stresses solutions provided by the model containing the spurious terms have been compared to stresses solutions provided by the corrected model. Those numerical analyses have demonstrated that the identified spurious terms are the cause of the model's locking, which delays convergence. Those analyses have also demonstrated the effectiveness of the procedure employed to eliminate the spurious terms.

In general, solutions provided by the corrected model converged monotonically and faster. Exceptions to this have been observed in the solutions of the in-plane shear stress τ_{xy} for both thicknesses of the angle-ply laminate, and in the solution of the transverse shear stress τ_{yz} for the lower thickness non-symmetric cross-ply laminate. In those solutions, convergence was not monotonic after removal of the parasitic shear terms.

Numerical solutions have shown that locking effects are stronger in the lower thickness plates'

solutions than in the higher thickness plates' solutions. This was expected because as shear strains are negligible in thin plates parasitic shear should be very pronounced. Further, numerical solutions have shown that the corrected model provides correct results as stresses results converge well within analytical solutions. Finally, numerical solutions have shown that mostly shear stresses solutions provided by the model containing the spurious terms might not converge adequately to the correct solutions as the results oscillate or might be completely erroneous in the qualitative sense. Thus, it can be concluded that it is advantageous to use strain gradient notation as spurious terms can be identified precisely *a-priori* and then eliminated definitely from the element's matrices. Also, results obtained here strongly indicate that refinement alone might not guarantee the elimination of locking, enforcing the need to apply a technique to remove spurious terms from finite elements. The simple procedure made available through the use of strain gradient notation is appealing, and might be used as an alternative to employing well-known procedures such as reduced-order integration techniques.

Acknowledgements

The authors would like to acknowledge the scholarship provided by CAPES (brazilian agency) to the second and third authors during his and hers master's degree studies, allowing this research work to be conducted.

References

- Aagaah, M.R., Mahinfalah, M. and Jazar, G.N. (2003), "Linear static analysis and finite element modeling for laminated composite plates using third order shear deformation theory", *Comp. Struct.*, **62**, 27-39.
- Abdalla, F^o JE Qualitative and Discretization Error Analysis of Laminated Composite Plate Models. Ph.D. Dissertation (1992), University of Colorado, Boulder, CO.
- Abdalla, F^o JE and Dow, J.O. (1994), "An error analysis approach for laminated composite plate finite element models", *Comput. Struct.*, **52**(4), 611-616.
- Ahamad, S., Irons, B.M. and Zienkiewicz, O.C. (1970), "Analysis of thick and thin shell structures by curved finite elements", *Int. J. Numer. Meth. Eng.*, **2**, 419-451.
- Bathe, K.J. and Dvorkin, E. (1985), "A four-node plate bending element based on Mindlin/Reissner plate theory and a mixed interpolation", *Int. J. Numer. Meth. Eng.*, **21**, 367-383.
- Bose, P. and Reddy, J.N. (1998), "Analysis of composite plates using various plate theories, Part 1: Formulation and analytical solutions", *Struct. Eng. Mech.*, **6**(6), 583-612.
- Bose, P. and Reddy, J.N. (1998), "Analysis of composite plates using various plate theories, Part 2: Finite element model and numerical results", *Struct. Eng. Mech.*, **6**(7), 727-746.
- Botello, S., Onate, E. and Canet, J.M. (1999), "A layer-wise triangle for analysis of laminated composite plates and shells", *Comput. Struct.*, **70**, 635-646.
- Brank, B. and Carrera, E. (2000), "A family of shear-deformable shell finite elements for composite structures", *Comput. Struct.*, **76**, 287-297.
- Dow, J.O. (1999), *A Unified Approach to the Finite Element Method and Error Analysis Procedures*, Academic Press, San Diego, CA.
- Dow, J.O. and Abdalla, F^o JE (1994), "Qualitative errors in laminated composite plate models", *Int. J. Numer. Meth. Eng.*, **37**, 1215-1230.
- Dow, J.O. and Byrd, D.E. (1988), "The identification and elimination of artificial stiffening errors in finite elements", *Int. J. Numer. Meth. Eng.*, **26**, 743-762.
- Dow, J.O. and Byrd, D.E. (1990), "Error estimation procedure for plate bending elements", *AIAA J.*, **28**, 685-693.

- Dow, J.O., Feng, C.C., Su, S.Z. and Bodley, C.S. (1985), "An equivalent continuum representation of structures composed of repeated elements", *AIAA J.*, **23**, 1564-1569.
- Dow, J.O., Ho, T.H. and Cabiness, H.D. (1985), "A generalized finite element evaluation procedure", *J. Struct. Eng.*, ASCE, **111**(2), 435-452.
- Dow, J.O. and Huyer, S.A. (1989), "Continuum models of space station structures", *J. Aerospace Eng.*, ASCE, **2**(4), 212-230.
- Ghugal, Y.M. and Shimpi, R.P. (2002), "A review of refined shear deformation theories of isotropic and anisotropic laminated plates", *J. Reinf. Plast. Comp.*, **21**(9), 775-805.
- Hughes, T.J.R., Cohen, M. and Haroun, M. (1978), "Reduced and selective integration techniques in finite element analysis of plates", *Nuclear Eng. Des.*, **46**, 203-222.
- Hughes, T.J.R., Taylor, R.L. and Kanoknukulchai, W. (1977), "A simple and efficient finite element for plate bending", *Int. J. Numer. Meth. Eng.*, **11**, 1529-1543.
- Lo, K.H., Cristensen, R.M. and Wu, E.M. (1977), "A high-order theory of plate deformation, Part 1: Homogeneous plates", *J. Appl. Mech.*, **44**(4), 663-668.
- Lo, K.H., Cristensen, R.M. and Wu, E.M. (1977), "A high-order theory of plate deformation, Part 2: Laminated plates", *J. Appl. Mech.*, **44**(4), 669-676.
- Prathap, G. (1997), "A field-consistency approach to plate elements", *Struct. Eng. Mech.*, **5**(6), 853-865.
- Reddy, J.N. (2004), *Mechanics of Laminated Composite Plates and Shells: Theory and Analysis*, 2nd ed., CRC Press, Boca Raton, FL.
- Reddy, J.N. (1989), "On refined computational models of composite laminates", *Int. J. Numer. Meth. Eng.*, **27**, 361-382.
- Reddy, J.N. and Averill, R.C. (1991), "Advances in the modelling of laminated plates", *Comput. Syst. Eng.*, **2**(5/6), 541-555.
- Reddy, J.N. and Wang, C.M. (2000), "An overview of the relationships between solutions of the classical and shear deformation plate theories", *Comp. Sci. Tech.*, **60**, 2327-2335.
- Sheikh, A.H. and Chakrabarti, A. (2003), "A new plate bending element based on higher-order shear deformation theory for the analysis of composite plates", *Finite Elem. Anal. Design*, **39**, 883-903.
- Singh, G. and Rao, G.V. (1995), "A discussion on simple third-order theories and elasticity approaches for flexure of laminated plates", *Struct. Eng. Mech.*, **3**(2), 121-133.
- Zienkiewicz, O.C., Taylor, R.L. and Too, J.M. (1971), "Reduced integration technique in general analysis of plates and shells", *Int. J. Numer. Meth. Eng.*, **3**, 275-290.